Characterization and development of FeCrW high speed steel coating for abrasive and impact wear applications

By

Dennis Rinkel

Diploma work No. 182/2016
At Department of Materials and Manufacturing Technology
CHALMERS UNIVERSITY OF TECHNOLOGY
Gothenburg, Sweden

Diploma work in the Master programme Materials Engineering

Performed at: Höganäs AB
                        Bruksgatan 35, Höganäs

Supervisor(s):   Barbara Maroli
                        Höganäs AB
                        Bruksgatan 35, Höganäs

Examiner: Sven Bengtsson
                        Department of Materials and Manufacturing Technology
                        Chalmers University of Technology, SE - 412 96 Gothenburg

Characterization and development of FeCrW high speed steel coating for wear and impact wear loaded applications
Dennis Rinkel

SUMMARY

XH-7 is a high speed steel alloy developed for use in surface coating to improve the impact and abrasive wear resistance of machine parts and tools. The desired structure of the material is a martensitic matrix with fine carbide and boride precipitates. In order to form these precipitates carbide forming elements such as: W, Cr, V, and Nb, are added to the alloy. It has been found that XH-7 has a tendency to form an area with a ferritic matrix phase when laser cladded.

The thesis has been performed in order to solve the problem of scatter in the microstructure of laser cladded XH-7. In order to achieve this the thesis is split into two parts characterization, and development.

During the characterization phase simulations, microscopy and mechanical testing is used to identify the phases present in XH-7, explain the solidification behaviour of the material, and explain the reason for the formation of the ferritic matrix. In this part of the thesis it was found that the softer ferritic matrix formed in the slowest cooling regions of the clad, while the faster cooling regions showed a martensitic matrix. Apart from the matrix phase both areas contained the same phases namely: NbC, W_2B, and a eutectic structure made up of either W_2B or $M_{23}C_6$, and fine grains of matrix phase. It was concluded that the ferritic matrix formed when the formation of NbC depleted the carbon content of the liquid. The reason this did not happen in the martensitic areas is caused by the high cooling rate which allowed austenite to begin solidifying before the carbon in the liquid had depleted significantly.

During the development phase several alternative alloys to XH-7 were developed. With the goal of preventing the formation of ferrite. The two most promising were labelled XH-7B and XH-7C.

Keywords: High speed steel, laser cladding, surface coating, alloy characterization.

Preface

I would like to thank Höganäs AB for giving me the opportunity me to perform my master's thesis at the company. I would especially like to thank my supervisor **Sven Bengtsson** and **Barbara Maroli** for their input, guidance, and support during my time at Höganäs. I have enjoyed working for you and feel like I have learned allot from both of you.

Contents

1 Introduction

Overlay welding is a welding procedure that places a weld metal clad on top of a base material. Generally, this is done to improve the wear or corrosion resistance of a part by cladding it with a different material compared to the base material.

The subject of this thesis is a new high speed steel alloy developed for use in laser cladding and plasma transferred arc welding.

X-H7 is an iron based alloy for overlay welding processes as laser cladding and plasma transferred arc welding. The alloy has a high hardness of around 65HRC and it is designed for applications requiring resistance to abrasive and impact wear. However, it was found that under certain conditions soft spots were formed during laser cladding. These soft spots are not found on PTA welded coatings. It is the goal of this project to find ways to avoid the soft spots while maintaining the wear and impact wear performance.

1.1 Goal and criteria

The goals of this thesis have been defined as:

- A deeper understanding of the development of the microstructure during the coating process.
- An in-depth understanding of factors influencing the microstructure and resulting coating properties.
- Identify chemical composition that provides a large process window and robust properties

1.2 Description of project

The thesis can be divided in two phases:

- The first phase is the characterization of the XH-7 material, this part focusses on:
  - Explanation of the behaviour of the material during solidification.
  - Identification of the phases present in laser cladded XH-7.
  - Identification and reason for the formation of the soft areas in laser cladded XH-7
- The second phase is the development new variants of XH-7 to resolve the problem of the soft areas.

2 Background

2.1 High speed steel

High speed steels (HSS) are defined as iron based alloys of carbon, chromium, vanadium, molybdenum, tungsten, or combinations of these. [1] This group of steels is named because of their main application is machining materials at high cutting speeds. The carbon and alloying elements used in these types of steel are used to give them high hardenability, wear resistance, hot hardness, and good toughness. Commercially there are two types of HSS defined:

- Standard HSS: Tool steels that serve almost all cutting conditions
- Intermediate HSS: Smaller group that are useable for more limited cutting conditions

The minimum requirements a material must meet to be classified as HSS are listed in Table 1.

Table 1. Minimum requirements for HSS classification [1]

Requirement	Standard	Intermediate
Carbon %	0,65	0,7
Chromium %	3,5	3,25
Vanadium %	0,8	0,8
Tungsten%	11,75	6,5
Minimum alloy content[1] for alloys containing >5% Co	22,5	13
Minimum alloy content[1] for alloys containing <5% Co	21	12
Ability to be austenitized and tempered at temperatures above 510°C	63HRC	62HRC

HSS alloys share some similarities in properties:
- High alloy content
- High enough carbon content to allow hardening to 64 HRC
- Uniform hardness throughout the entire cross-section
- High temperature hardening and martensite start temperature high enough to allow cooling in air.
- Possess high amount of carbide/boride/nitride particles that contain a high amount of the alloying elements.

2.1.1 Alloying elements in HSS

The most commonly added elements added to HSS and their intended effects are [1] [2]:

Carbon: Carbon is the most important element and is usually tightly controlled. Variations in the carbon content can have large consequences for the mechanical properties and microstructure of the alloy. Rising carbon content will increase hardness and strength, decrease the martensite start temperature and increases the amount of formed carbides. These carbides contribute to the hardness and wear resistance of HSS.

Silicon: Silicon has a small effect up to 1 wt%. Increasing the Si content raises the hardness but also slightly lowers the toughness. Another effect of alloying with silicon is an increased

---

[1] $(\frac{1}{3}Cr + 6,2V + W + 1,8Mo)$

solubility of carbon into the matrix, it also promotes the formation of M_6C carbides but does not affect the distribution of carbides.

Manganese: Manganese increases strength and hardness but increases the brittleness. This element is not normally used in large amounts in HSS because the increased brittleness increases the chance of cracking during quenching. Manganese also influences the amount of retained austenite.

Chromium: Chromium is added to HSS in quantities between 3 and 5% and is mainly added for its hardening effect and for the formation of carbides $Cr_{23}C_6$ and Cr_7C_3. A different effect of chromium is to shrink the austenite forming area and the stabilizing of ferrite.

Tungsten: Tungsten is found in almost all high speed steels. It is used to form hard carbides that significantly increase wear resistance and improves hot hardness, resistance to tempering, and causes secondary hardening. If the tungsten concentration is decreased, it is usually replaced by molybdenum.

Molybdenum: molybdenum forms the same carbides as tungsten does, however since it has about half the atomic weight it can replace tungsten by a factor of 1 Mo for 2 W. Because the melting point for molybdenum is lower than that of tungsten molybdenum alloys also have a narrower hardening range. Molybdenum alloys have a higher toughness than tungsten alloys but have a lowered hot hardness. In order to improve the hot hardness most molybdenum HSS alloys also have an addition of tungsten and vanadium.

Vanadium: Vanadium is added for its ability to form very hard stable carbides, these carbides greatly improve the wear resistance and slightly raise the hot hardness.

Cobalt: Cobalt is added to HSS to increase the hot hardness. Alloying with cobalt raises the liquidus temperature and thus gives a higher austenisation temperature allowing more carbides to be dissolved and resulting in more retained austenite. This latter effect is slightly compensated by also decreasing the stability of austenite and raising the martensite start temperature.

2.2 Martensite formation

When steel is quenched rapidly enough from the austenitic field it transforms into martensite. This diffusionless transformation occurs when there is not enough time for diffusion controlled processes to occur. Martensite is a term used in metallurgy for any product of diffusion less transformation, a transformation where the movement of atoms is less than one interatomic spacing. In steels, martensite is formed when the cooling rate is high enough that the carbon atoms in solution in the fcc γ-Fe stay in solution in the bcc α-Fe forming a saturated solid solution of carbon in α-Fe normally designated as α'.

2.2.1 Martensite growth

The martensite phase (α') is often formed in the shape of a lens and initially spans an entire grain diameter. More martensite forms by transforming the remaining austenite between the plates that have already been formed. The transformation of martensite starts at the "martensite start temperature" (M_S). The martensite finish (M_F) temperature shows the temperature where more cooling does not increase the amount of martensite. In practice this does not mean the material has fully transformed as there will always be some retained austenite.

The martensite transformation starts when the free energy barrier to nucleation (ΔG^*) is overcome. The value for this term is given by the following equation:

$$\Delta G^* \left(\frac{J}{nucleus} \right) = \frac{512}{3} * \frac{\gamma^3}{(\Delta G_v)^4} * \left(\frac{s}{2} \right)^4 * \mu^2 \pi \quad [3]$$

Equation 1. Free energy barrier to nucleation

Where:

γ = the coherent interfacial energy of the coherent nucleus
ΔG_V = the volume free energy release
s = shear strain
μ = Shear modulus of austenite
The critical nucleus size (c*=thickness and a*=radius) required for the formation of martensite can be calculated by:

$$c^* = \frac{2\gamma}{\Delta G_V}$$
$$a^* = \frac{16\gamma(s/2)^2}{{\Delta G_V}^2} \quad [3]$$

Equation 2. Critical nucleus size

It can be seen from these equations that both ΔG* and the critical nucleus size are dependent on ΔG_V, s, and γ.

After ΔG* has been reached the ΔG_V becomes so high that the required critical radius becomes low enough for martensite plates to start growing rapidly until they hit a high angle grain boundary or a different martensite plate. At first thin plates with high a/c ratios will form which will thicken after formation. In medium to high carbon steel this leaves a "midrib" of fine twins with an outer region of regularly arranged dislocations. Low carbon steel contains a high dislocation density, sometimes arranged as a cellular structure instead of twins. High carbon steel contains only twins.

2.2.2 Transformation temperatures

The martensite start temperature can be estimated using the following formula:

$$Ms\ (°C) = 545 - 330C - 2Al + 7Co - 14Cr - 13Cu - 23Mn - 5Mo - 4Nb - 13Ni - 7Si + 3Ti + 4V \quad [4]$$

Equation 3. Martensite start temperature

2.3 Laser cladding

Laser cladding is a surface coating technique wherein a high energy density laser is used as a heat source. The process is used to coat a metallic surface with a different metallic material. The area to be cladded is heated through absorption of energy delivered by a high power laser beam. Because laser light is highly monochromatic and directional it allows focussing of the laser into a very high power density. Because of the high power density the energy can be focussed on a specific point on the surface of the substrate, this results in a relatively low heat input into the substrate material compared to other processes. The low heat input has minimal effect on the substrate which allows laser cladding to be used on both thick and thin parts. [5]

Despite having low heat input into the substrate the heat input into the focus point is extremely high causing high heating rates on the surface. After the heat source has moved away diffusion of heat into the cold material causes the heated area to self-quench. This high heating and cooling rate causes: A refinement of the microstructure and in some cases the formation of metastable phases.

The laser cladding process can be modified by varying one or more of the process parameters. The most important parameters in laser cladding are: Laser power, beam size, beam manipulation methods, travel speed, powder feed method, and powder feed rate. The effect of adjusting the parameters is shown in Table 2.

Table 2. Influence of increased process parameters on clad properties [6]

Parameters	Clad height	Melt depth	Geometrical dilution	Hardness /cracking	Clad width
Laser power	-	+	+	-	+
Feed rate	+	-	-	+	-
Quantity of coating material	+	-	-	+	+
Laser spot size	+	-	-	+	-

Powder is blown directly into the melt pool by a carrier gas at an angle of 38-45°. The particles are heated as they pass through the laser beam and melt when they reach the melt pool. In order to prevent high dilution it is important that the laser power is high enough to melt the clad material without melting too much of the substrate. [1]. Powder that strikes the substrate surface instead of the melt pool is deflected. This method can be used to produce a high quality cladding with low dilution. Figure 1 shows a schematic representation of the coaxial-fed powder laser cladding process used at höganäs.
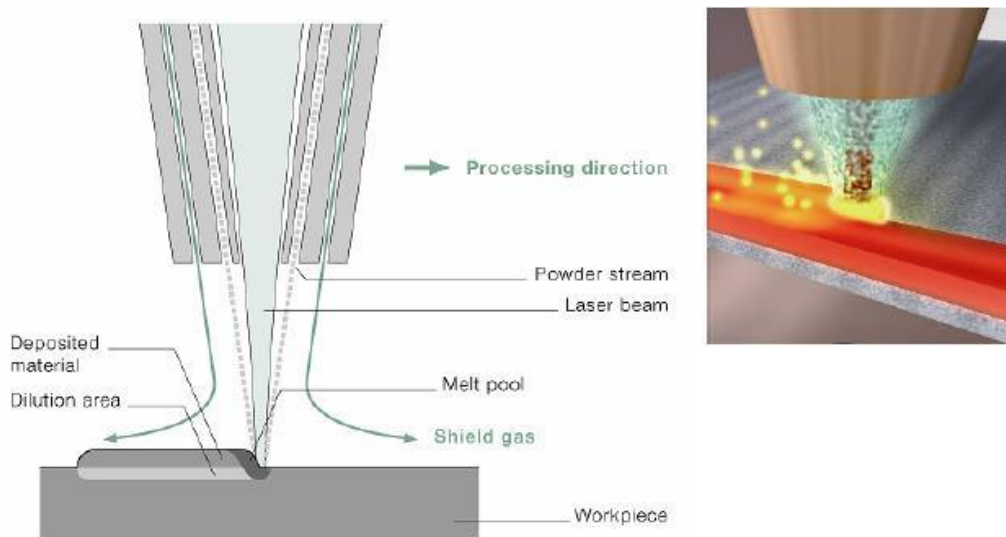

Figure 1: Coaxial-fed powder laser cladding process, Image supplied by Höganäs

2.4 Plasma Transferred Arc overlay welding

Plasma transferred arc welding is a coating method for metallic surfaces. The principle behind PTA welding is the formation of an electric arc between a non-consumable tungsten electrode and the substrate materials to create a melt pool. This arc is established by ionised plasma gas

---

[1] $Dilution(\%) = \frac{Clad\ depth}{Total\ clad\ height} \times 100$

between the electrode and the substrate. Filler material is fed into the arc either in wire or powder form to create a metallurgical bond with the substrate.

2.5 Comparison between PTA and Laser cladding

When these two deposition techniques are compared it can be said that PTA has a higher total heat input per kg of deposited material than laser cladding. This results in higher dilution, larger heat affected zone, lower cooling rate, and a generally a coarser microstructure.

2.6 Description of the material

XH-7 is a high speed steel alloy developed for use in surface coating to improve the impact and abrasive wear resistance of machine parts and tools, for example in industries like agriculture and mining. The desired structure of the material is a martensitic matrix with fine carbide and boride precipitates. Large hard particles are not desired as they would increase brittleness. Higher carbides and borides like $M_{23}C_6$ are not desired due to their lower hardness and poor wear and abrasive properties. Carbide and boride forming elements such as: W, Cr, V, and Nb, are added to the alloy. In order to provide sufficient hardenability to the matrix an abundance of solution hardening elements like: W, Cr, and Si are also added.

2.6.1 Soft areas

It has been found that XH-7 has a tendency to form an area with a soft matrix phase when laser cladded. Figure 2 shows a typical etched cross section of laser cladded XH-7, the dark areas are the softer areas. Figure 3 shows the softer dark area in higher magnification, while Figure 4 shows the harder light area, also in higher magnification.
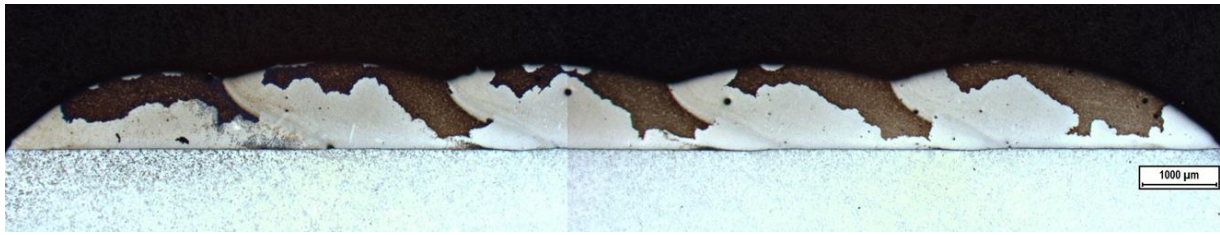
Figure 2. Typical example of etched laser cladded XH-7, The dark area shows significantly lower hardness than the light area. Etched in 3.3.
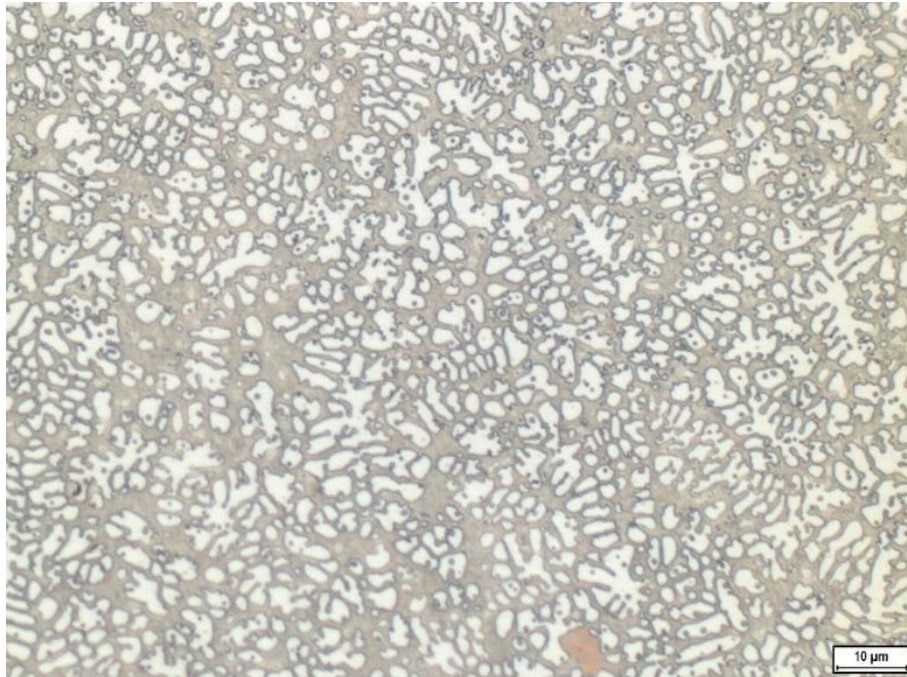

Figure 3. Microstructure of dark area in Figure 2, etched in 3.3

Figure 4. Microstructure of light area in Figure 2, etched in 3.3

3   Phase 1

The first phase of the thesis is concentrated on the characterization of XH-7 clad. Characterization is performed to receive information on the microstructure and properties of the XH-7 material.

3.1   Experimental

3.1.1   Material

The XH-7 material used in these experiments is an atomized powder, the composition of this is shown in Table 3. The particle size range of the powder used for overlay welding is 53-150μm.

Table 3. Chemical composition of XH-7

Composition (wt%)						
Fe	C	Cr	Nb	Ti	W	Other
Bal	<1	<5	<2	<1	<10	<7

3.1.2   Cladding conditions

The powder was cladded by PTA and laser. Hettinger PTA was used for the experiments. For laser cladding two different type of lasers were used: direct diode laser, and a fibre laser. Varying process parameters were used to clad the material. The parameters that were altered are: Laser spot size, cladding speed, laser power, and deposition rate. These parameters where used to produce clads with different heights, widths, dilution, and single or multiple track and layers. The parameters used can be found in Appendix 1.

3.1.3   Simulation of solidification

The solidification properties of the samples are simulated using the program "Thermo-Calc". The program version used was 3.1 and the database was TCFE6.

3.1.4   Metallography

The alloys that are examined for this thesis were cladded unto a low alloyed carbon steel and then a cross section was cut perpendicular to the cladding direction for further examination. The cross section was mounted in Bakelite, grinded and polished as follows:

- Al_2O_3 grinding stone until a flat surface is achieved
- 6 minutes on a 9μm cloth
- 6 minutes on a 3μm cloth
- 0,5 minutes on a 1μm cloth

After polishing the samples were etched to reveal the microstructure. The composition of the etchant used was:

- 100ml, 95% ethanol
- 1ml, concentrated hydrochloric acid
- 2g, picric acid

This etchant is called 3.3 and was used because earlier studies performed at Höganäs AB have shown that it was the most effective.

3.1.5   Microstructure analysis

The microstructure of the alloys discussed in this report was studied using light optical microscopy, scanning electron microscopy, and energy-dispersive X-ray spectroscopy.

The microscopes used are:
- Leica DM6000 light optical microscope
- Hitachi SU6600 SEM, equipped with bruker SDS detector for chemical analysis.
- Hitachi TM3030 tabletop SEM

The hardness of the samples was measured using a "Matzusawa MM-7 micro Vickers hardness tester" the hardness has been tested using a 100g weight. The values given in this report are an average of at least 6 measurements taken in an area.

In order to identify the soft phase formed in the XH-7 alloy an EBSD analysis was performed at Chalmers University of Technology. This method is used to characterize the grain orientation, and phases of crystalline materials. This method has been used to identify the crystal structure of the soft matrix in XH-7.

3.1.6 Heat treatment

This experiment was performed to characterize the microstructure of the soft areas found in the XH-7 laser cladded coatings. This was done by heating the samples to the austenitization temperature followed by cooling them to room temperature. Two cooling methods have been used one where the samples were left to cool in the furnace and one where the samples were cooled rapidly in oil. The samples selected for this experiment are XH-7 clads from the N series Appendix 1. The parameters of the heat treatment are shown in Table 4.

Table 4. Heat treatment parameters

Samples	Temperature	Time	Cooling
N18, N19, N20	1000°C	60 minutes	In furnace
N36, N37, N38	1000°C	60 minutes	In oil

All samples have been heated to 1000°C in a furnace with a nitrogen atmosphere. After one hour, samples N18, N19, and N20 were left to cool in the furnace for one hour, samples N36, N37, and N38 were cooled in an oil bath.

3.2 Results

3.2.1 Simulation

The microstructure of XH-7 was simulated using the program "Thermo-calc". In this chapter the results of these simulations performed for the XH-7 material will be discussed.

Simulation of the phase diagram of the XH-7 alloy has been performed using Thermo-Calc, the results of this simulation can be seen in Figure 5. The vertical black line has been added to designate the carbon content present in XH-7.
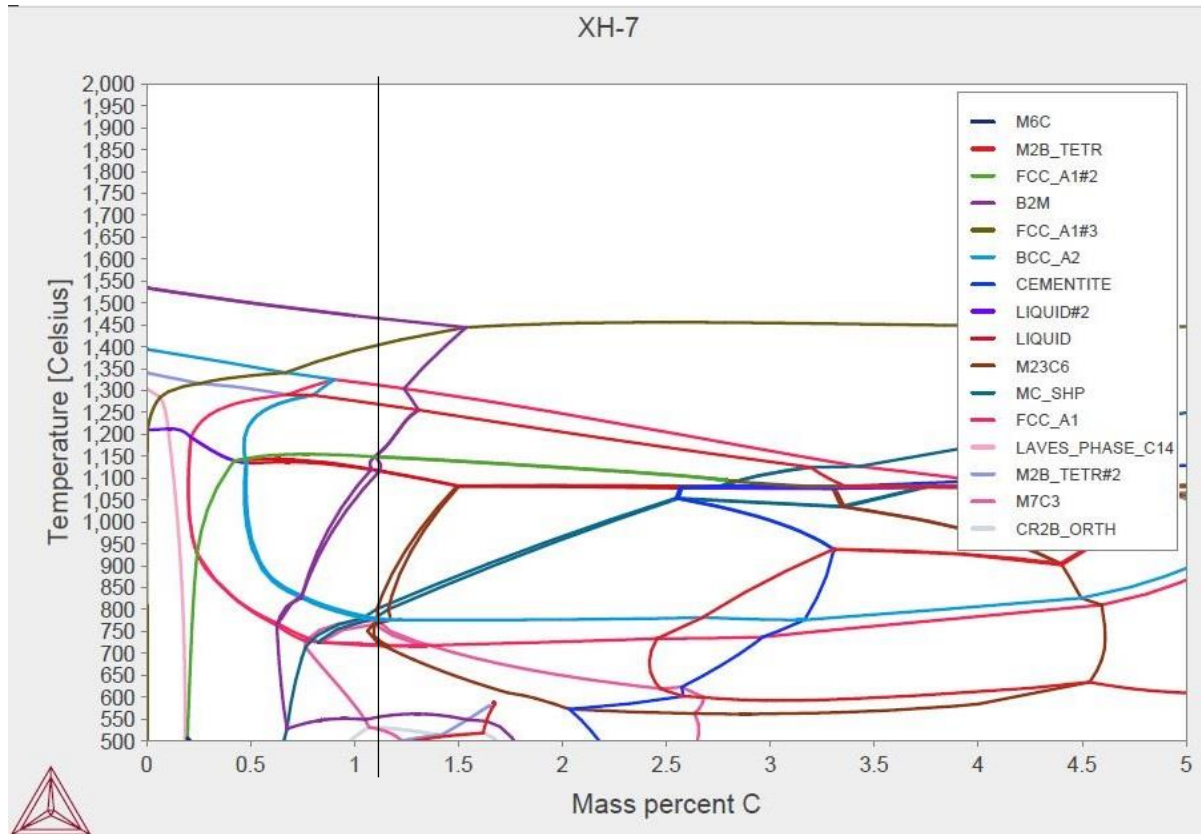

Figure 5. Simulated phase diagram XH-7

When the black line in Figure 5 is followed the following phase are expected to form: First at 1470°C a boride (B2M) is formed which is stable until 1100°C. Next at 1400°C a carbide (FCC_A1#3) is formed. At 1300°C austenite (FCC_A1) forms. At 1250°C a Boride (M2B_tetr#2) forms. At 1150°C a carbide (FCC_A1#2) form. At 1120°C al liquid has solidified.

The amount of each phase at different temperatures can be seen in Figure 6. The amount of B2M phase is multiplied by 10 in this figure because the highest amount formed is only 0,22Vol%, the amount of FCC_A1 and the liquid has been divided by 10. The composition below the solidus at 1000°C and 1.1% carbon of these predicted phases can be found in Table 5.
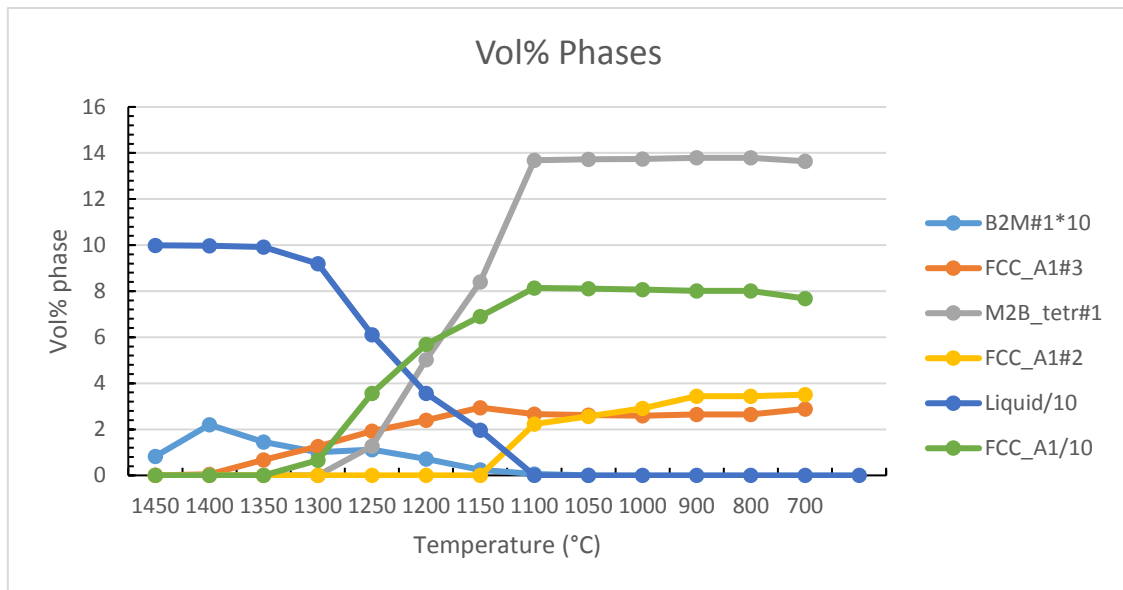
Figure 6. Vol% Phases as function of the Temperature (°C), simulated using Thermo-Calc 3.1

Table 5. Predicted phases and their composition at 1000°C, simulated using Thermo-Calc 3.1

Phase	Vol%	Mass fraction alloying element (Wt%)							
		Fe	C	B	Cr	Nb	Ti	W	V
FCC_A1#1	80,7	92,7	0,6	0,0	2,8	0,0	0,0	0,7	0,2
FCC_A1#2	2,9	3,6	14,1	0,0	5,8	9,0	2,6	18,4	46,5
FCC_A1#3	2,6	0,8	12,8	0,0	2,7	57,8	9,9	6,9	9,1
M2B_tetr#1	13,8	37,0	0,0	5,8	7,0	0,0	0,0	50,3	0,0

At 1000°C and 1,1% carbon four phases are predicted:

- FCC_A1#1: Austenite matrix containing 0,6% Carbon, If Equation 3 is applied to this composition the martensite start temperature would be 267°C.
- FCC_A1#2: Vanadium based carbide with high solubility of niobium, chromium, and tungsten, and a moderate amount of titanium.
- FCC_A1#3: Niobium based carbide with high solubility of titanium, tungsten and vanadium.
- M2B_tetr#1: Tungsten boride containing a high amount of iron and a moderate amount of chromium.

3.2.1.1 Scheil solidification diagram

The simulated Scheil diagram of the XH-7 alloy is shown in Figure 7. The Scheil diagram provides information about the solidification behaviour of the alloy and which phases are formed.
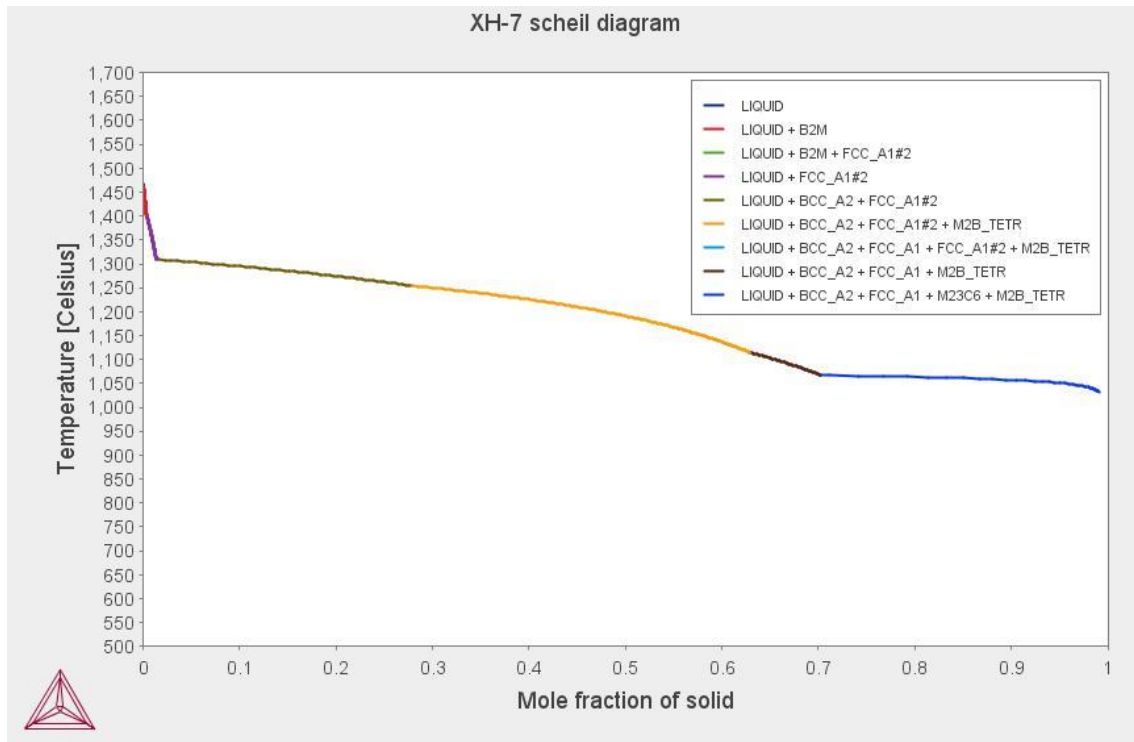
Figure 7. XH-7 Scheil diagram simulated using Thermo-Calc 3.1

The Scheil diagram predicts that:

- At 1450°C a boride (B_2M) is precipitated.
- At 1400°C A carbide (FCC_A1#2) is precipitated along with the boride.
- At 1300°C ferrite (BCC_A2) forms along with the carbide.
- At 1250°C a boride (M2B_tetr) forms, along with the ferrite and carbide
- At 1100°C austenite (FCC_A1) start to form along with the ferrite and boride.
- Finally at 1070°C a carbide (M23C6) forms and the last of the liquid solidifies around 1040°C.

3.2.1.2 Phase diagram vs Scheil diagram

If the result of the phase diagram is compared to the result of the Scheil diagram the most important differences are the formation of ferrite instead of austenite and the formation of a higher carbide (M23C6) in the last stage of solidification.

The reason for these differences is probably caused by the change in composition of the liquid as the matrix and carbides begin to solidify. Figure 8 shows the changing carbon content of the liquid vs the temperature, calculated supposing that equilibrium conditions are achieved during solidification. Figure 9 also shows the changing composition of the liquid during solidification, important to notice is the strong increase of the ferrite stabilizing elements chromium and vanadium.
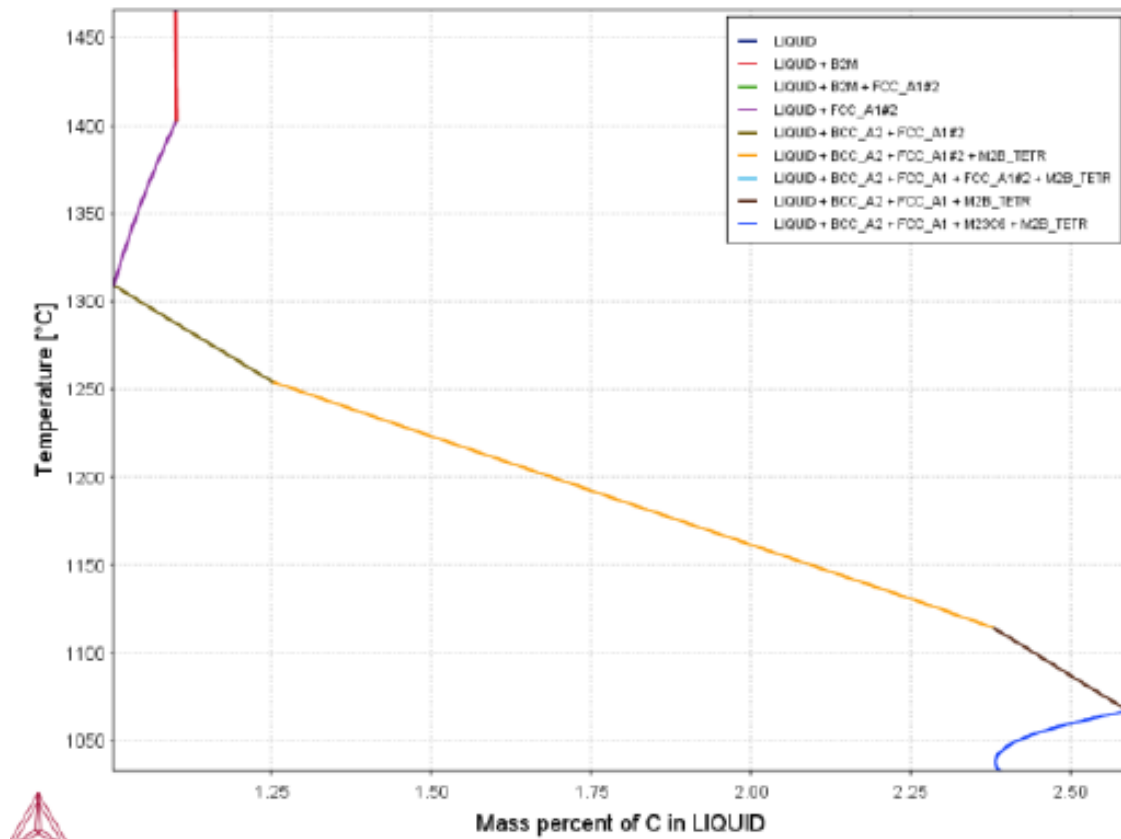
18

Figure 8. Carbon content of liquid at different temperatures

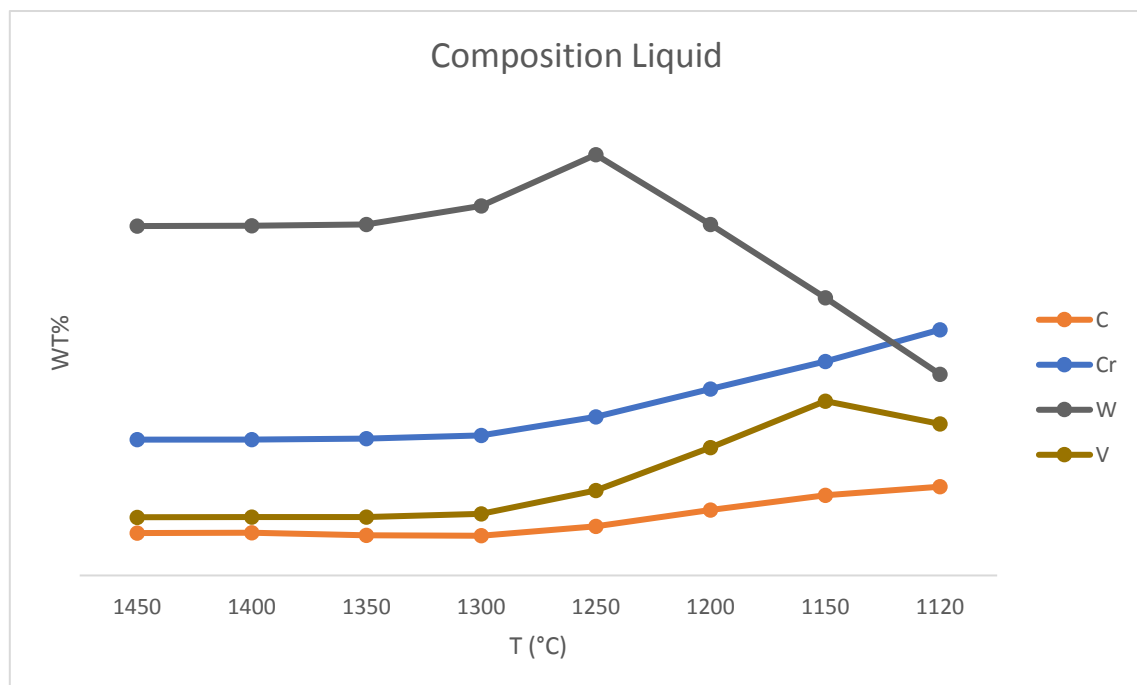*Figure 9. Changing composition of liquid with the temperature, data taken from Thermo-Calc simulation.*

3.2.2 Microstructure analysis XH-7

Microscopic examination of laser cladded XH-7 alloy was performed to characterize the microstructure of XH-7. This was done through a combination of light optical microscopy, SEM and EDS. Because two distinct areas can be distinguished after etching in 3.3 these areas will

be described separately. Figure 10 shows a typical cross-section of XH-7. The image shows two areas, a darker and lighter one. Measurements show that the light area is considerably harder than the dark area, 940HV compared to 600HV. The difference in colour is probably caused by the difference in effectiveness of the etchant causing the softer area to be etched slightly deeper than the harder area. Interesting to note is that the dark area always forms near the top surface of the clad, this is the area of the clad that is cooled slowest and solidifies last.
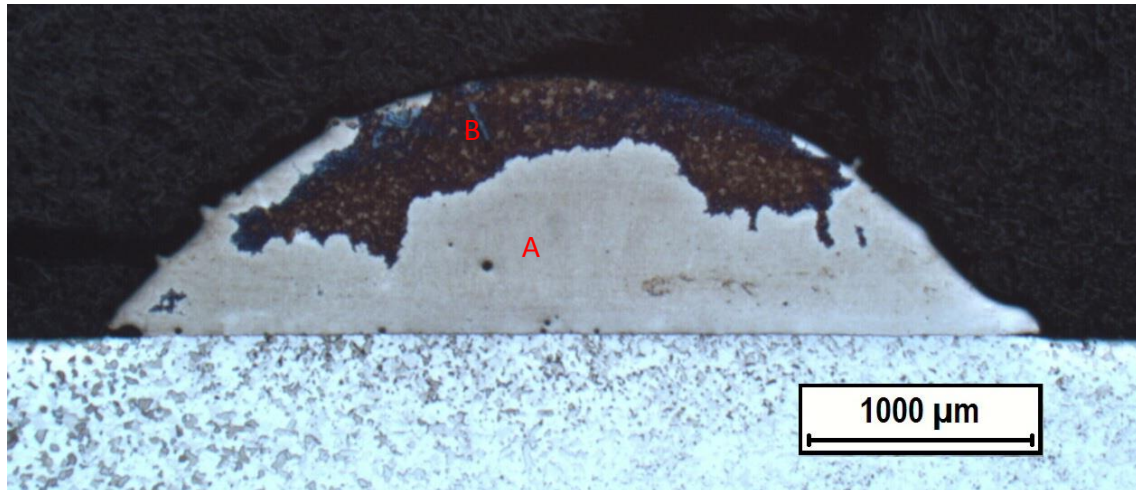
Figure 10. XH-7, sample: N2. Two clearly distinguishable areas can be seen (A) a lightly etched area, and (B) a more strongly etched area.

3.2.2.1 Microstructure of light area

Figure 11 shows the hard light area found in the XH-7 alloy. Three phases can be distinguished in this area independently of which sample was investigated.

1. A hard matrix consisting of cellular and dendritic martensite
2. A eutectic structure between the martensitic matrix
3. Small round carbides.

Figure 11. XH-7, Sample N35, microstructure of light area etched in 3.3. Martensitic primary dendrites (1), eutectic structure (2) and carbide or boride particles (3) are observed.

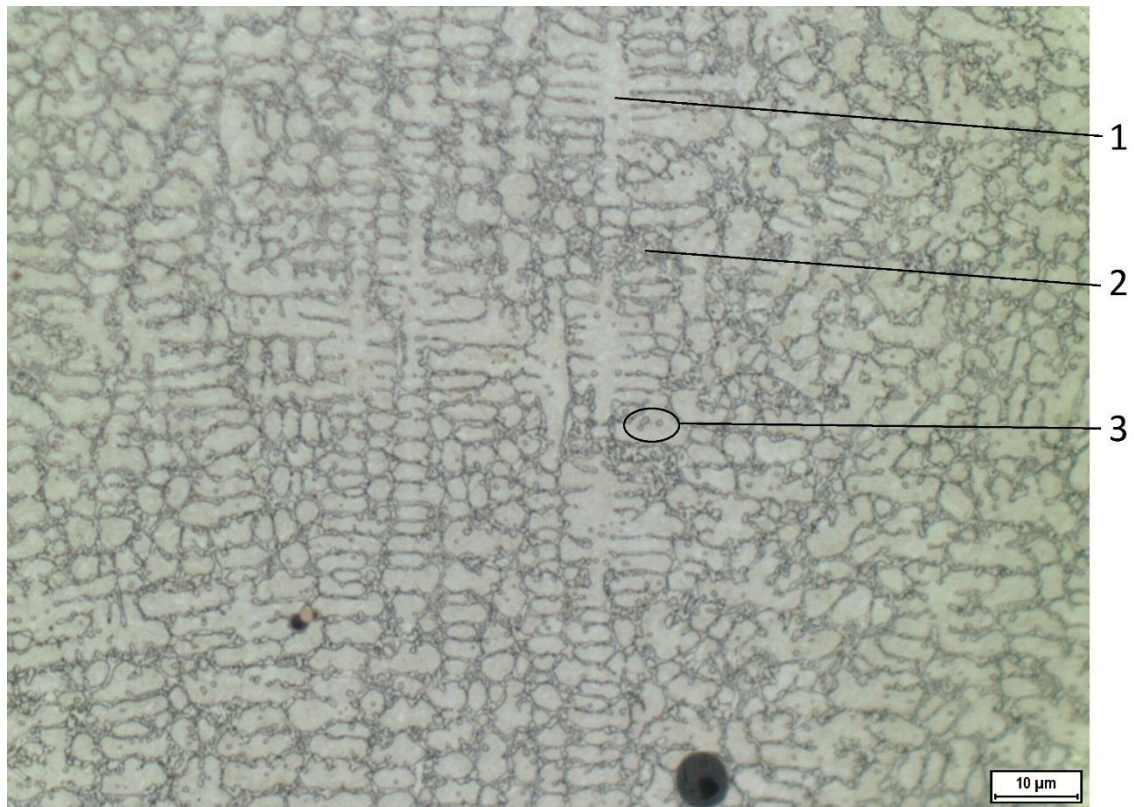Figure 12 shows a SEM image of a XH-7 clad at higher magnification, Figure 13 shows an EDS mapping of the elements present and Table 6 shows the measured composition of the phases found. Four phases can be distinguished:

1. A martensitic matrix, this matrix phase consists mainly of iron but also contains amounts of chromium, tungsten, niobium and silicon. There also measured are high amounts of carbon and boron, but because these elements have very low characteristic energy (>500 eV) these values can be unreliable due to the difficulty in analysing them by EDS.
2. A grey intercellular/interdendritic phase containing high amounts of vanadium, tungsten, niobium and iron. At high magnification this phase appears to be made up of a mixture of two different phases but because of the fineness of these phases it is difficult to resolve them.
3. A white intercellular/interdendritic phase consisting mainly of tungsten, with a contribution of chromium, and vanadium. This phase also shows a high signal for boron, which indicates a boride. Combined with the information obtained in Thermo-Calc this phase is identified as the M_2B_tetr.
4. Dark particles with a grey shell. The EDS map shows that these particles have a strong signal of niobium and a slightly weaker signal for titanium in the centre, this can be seen in figure 14. Figure 15 shows a line measurement along the diameter of one of these particles in this figure it can clearly be seen that the titanium signal increases near the centre of the particle and decreases near the edges.
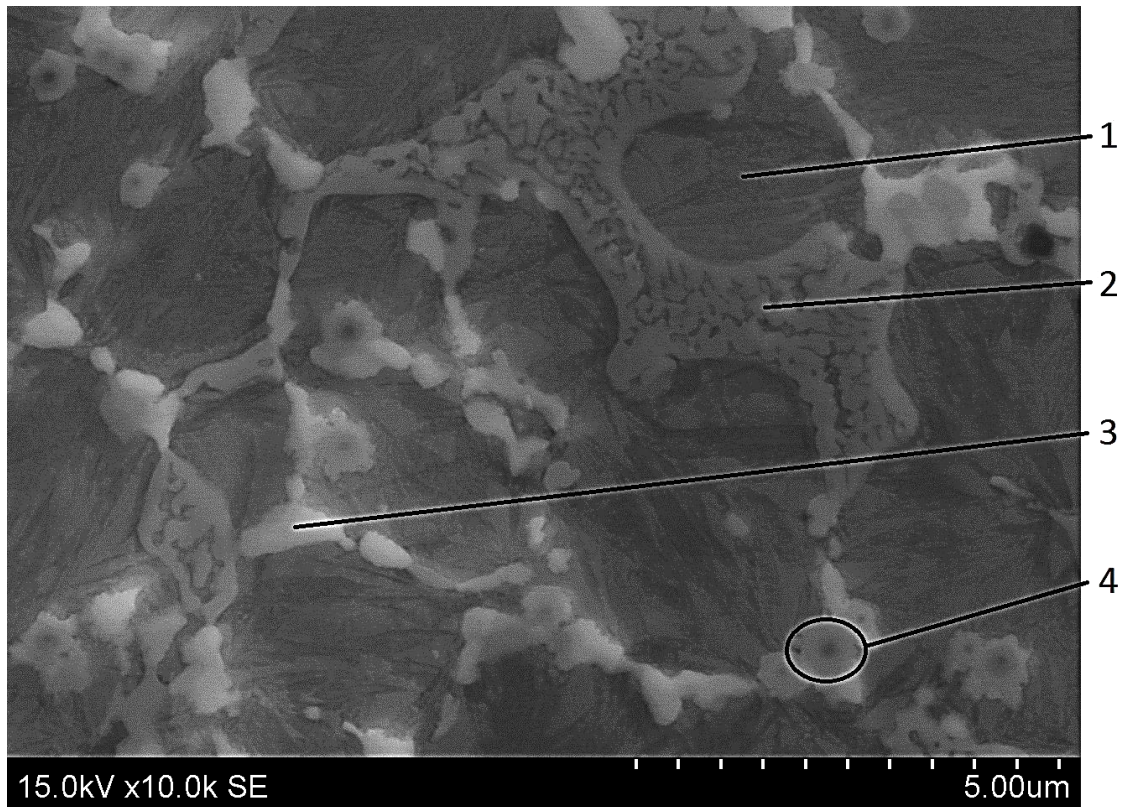
Figure 12. XH-7 light area etched in 3.3 as observed by SEM. Four different phases are identified martensite (1) eutectic (2), tungsten rich boride (M2B) (3), titanium and niobium rich precipitate

Table 6. Chemical composition of the phases identified in the light area measured by EDS analysis

Phase	Wt%							
	B	C	Ti	V	Cr	Fe	Nb	W
1	1,3	1,9	0,9	2,3	2,7	80,6	1	5,6
2	2,0	3,2	0,1	2,8	5	70,5	0,8	12,9
3	4,0	2,4	0,0	6,6	5,6	37,7	1,5	41,2
4	5,7	9,1	3,0	3,7	2,5	18,4	37,1	18,6

Figure 13. EDS Map XH-7, Light area, etched using 3.3

Figure 14. Figure 12, EDS map of Ti and Nb

Figure 15. Line measurement along diameter FCC_A1#2

3.2.2.2 Microstructure of dark area

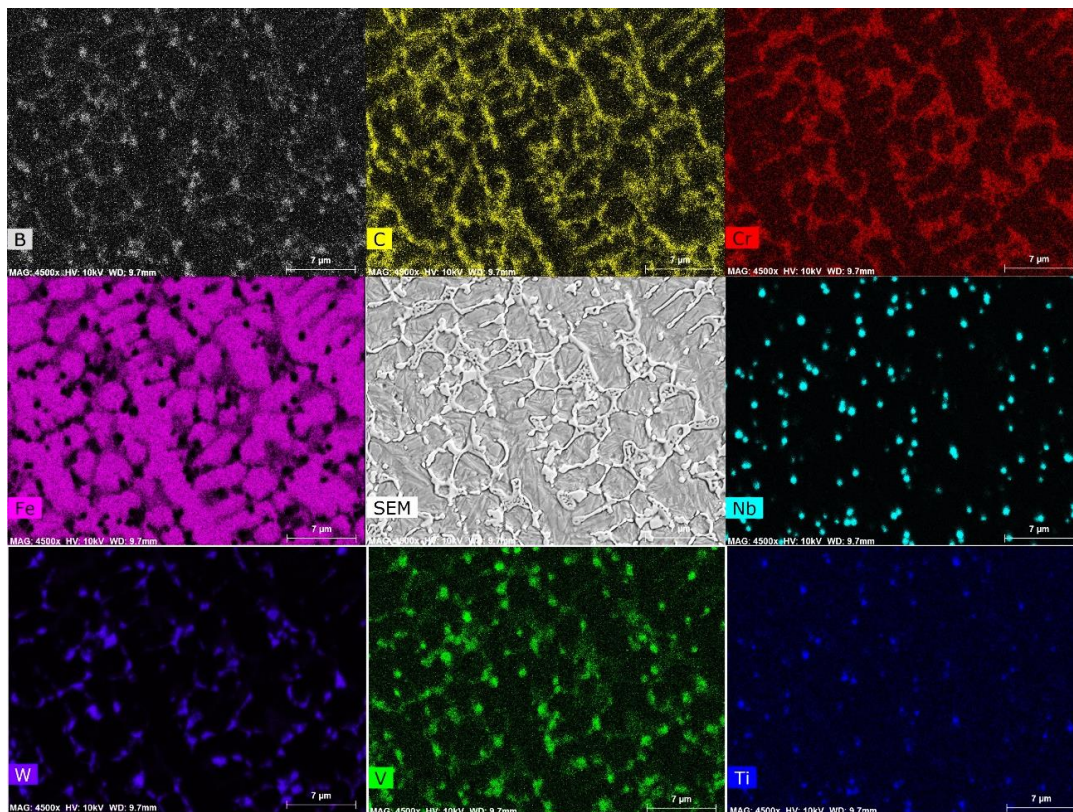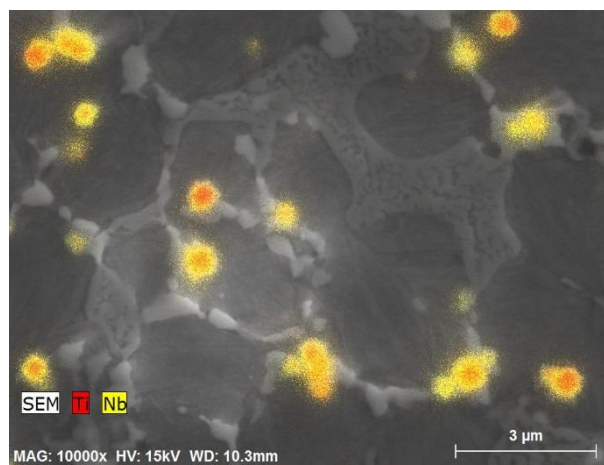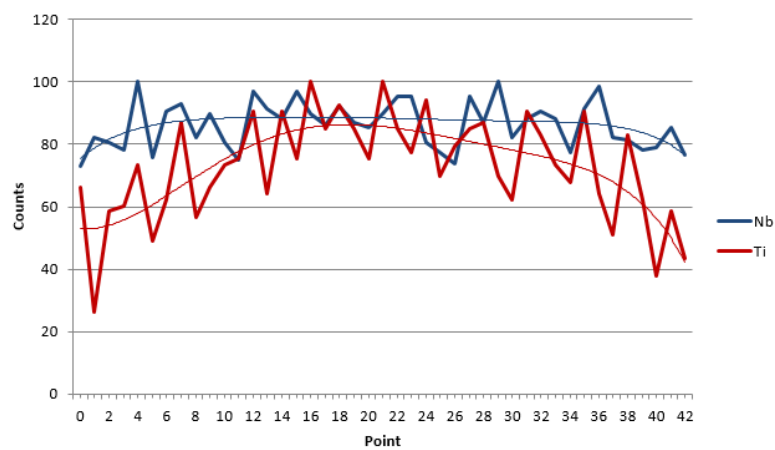Figure 16 shows the soft dark area found in the XH-7 alloy as observed under a light optical microscope. Three phases can be distinguished.

1. A soft matrix consisting of ferritic or austenitic dendrites.
2. A eutectic structure between the matrix phase.
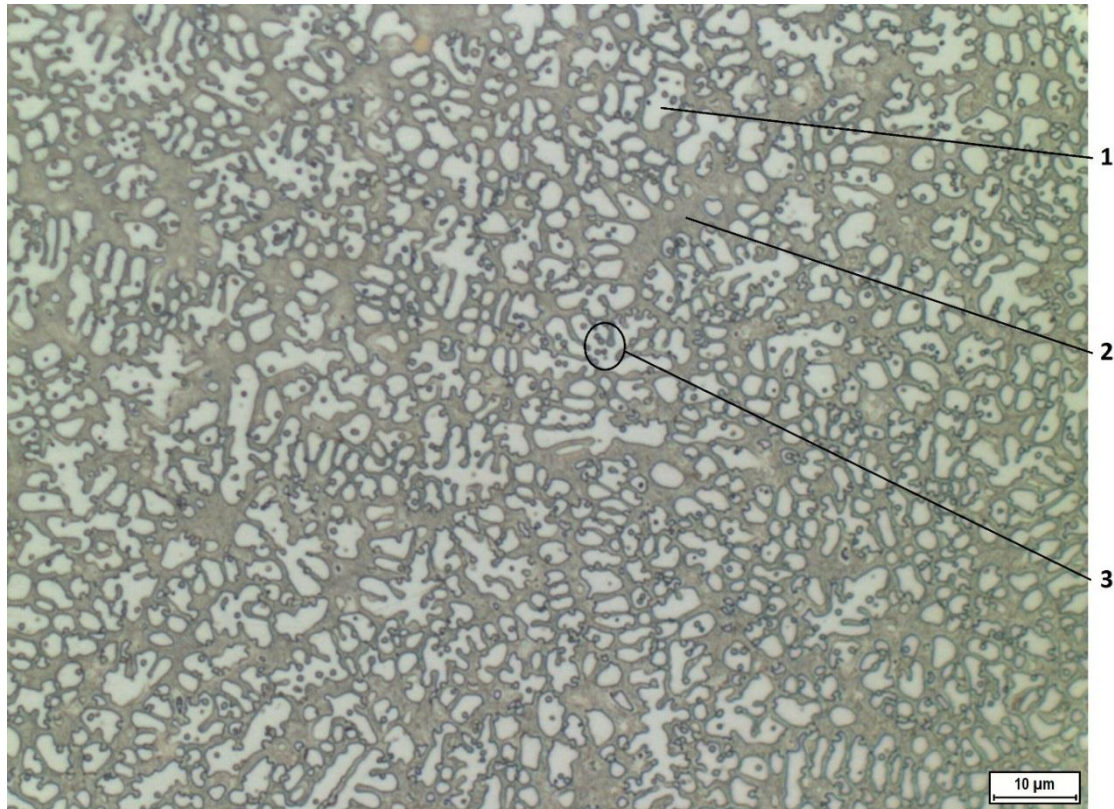3. Small round precipitates.

Figure 16. XH-7, Sample: N35 dark area

Figure 17 shows the microstructure of a XH-7 clad as observed by SEM, Figure 18 shows an EDS mapping of the elements present in XH-7. Four phases can be distinguished:

1. A matrix phase consists mainly of iron but also contains amounts of chromium, tungsten, niobium and silicon. Hardness measurements show that unlike the light area this phase is not martensite, it is assumed that this phase is either ferrite or austenite. The EDS analysis shows a high amount of boron and carbon, but because these elements have very low characteristic energy (>500 eV) these values can be unreliable due to the difficulty in analysing them.
2. A white intercellular phase consisting mainly of tungsten, with a contribution of chromium, and vanadium. This phase also shows a high signal for boron, which indicates a boride. Combined with the information obtained in Thermo-Calc this phase is identified as the M_2B_tetr.
3. A grey intercellular phase containing high amounts of vanadium, tungsten, niobium and iron. At high magnification this phase appears to be made up of a mixture of two different phases but because of its fineness it is difficult to identify this phase.
4. Dark particles with a grey shell. The EDS map shows that these particles have a strong signal of niobium and a signal for titanium in the centre, an example of this can be seen in figure 14. Figure 15 shows a line measurement along the diameter of one of these

particles, this figure also shows an increase in signal strength for titanium towards the centre. Combined with the information received from the Thermo-Calc simulation it is believed that this phase first formed as titanium boride (B2M) which then acted as a nucleation site for niobium carbide ((FCC_A1#2).
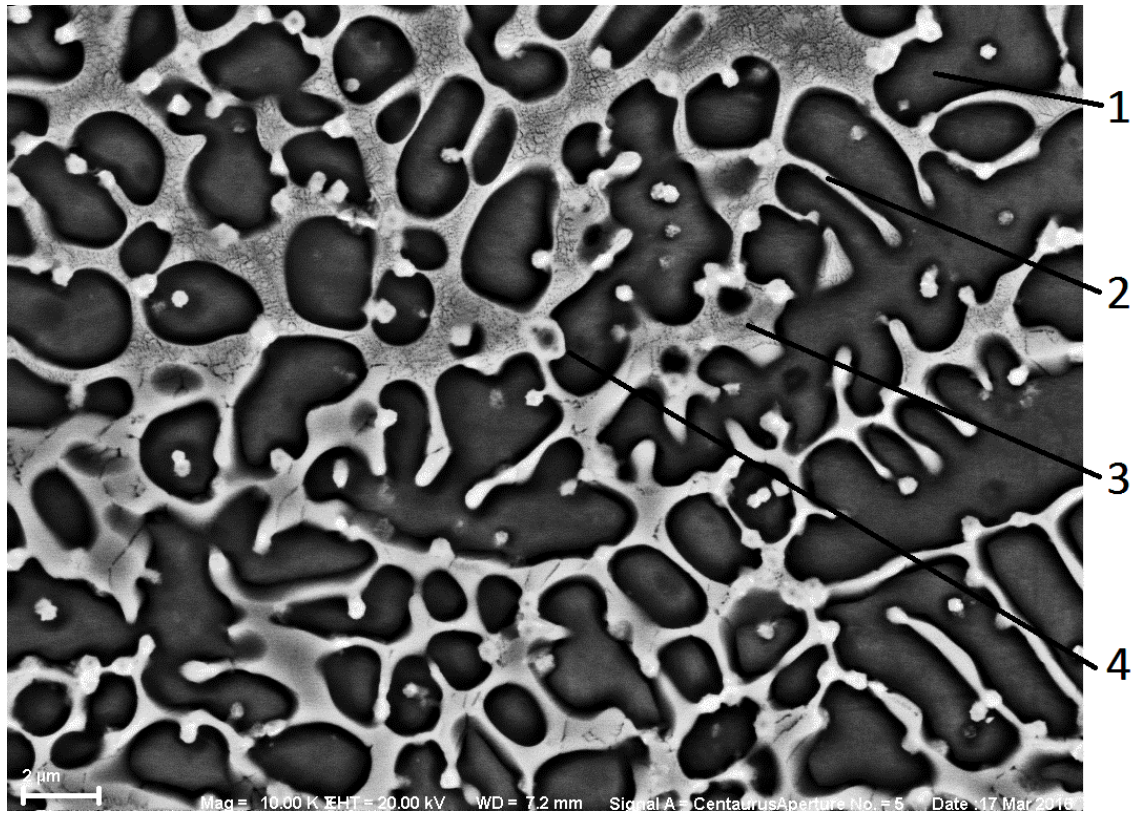
Figure 17. XH-7, sample: N32 dark area

Table 7. Measured composition dark area

Phase	B	C	Si	Ti	V	Cr	Mn	Fe	Nb	W
					Wt%					
1	1,4	1,7	0,8	0,2	1,4	2,6	2,5	85,1	0,7	5,1
2	4,3	2,4	0,0	0,0	3,8	5,4	2,1	57,5	1,7	23,8
3	2,1	3,0	0,0	0,0	2,4	5,2	2,8	74,7	0,4	11,4
4	3,2	8,2	0,0	9,2	3,7	1,2	1,0	21,9	40,0	11,6
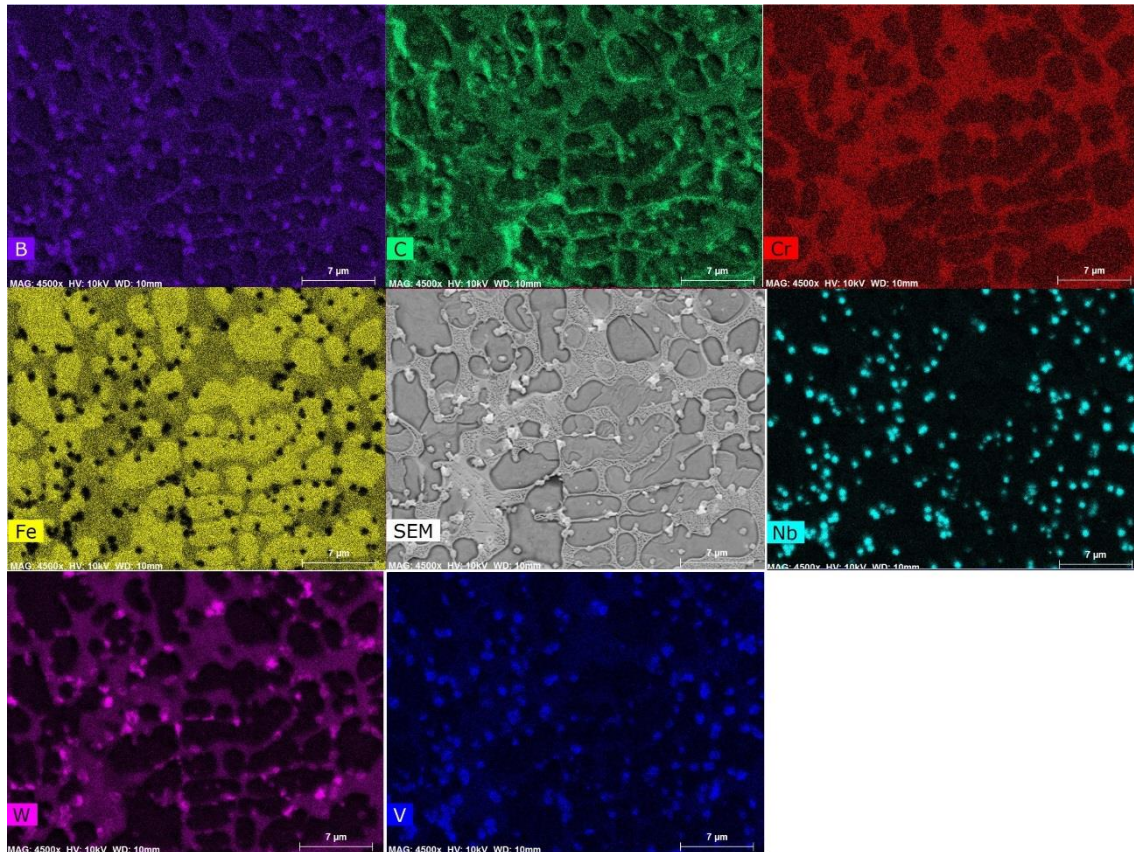
Figure 18. EDS Map XH-7, Dark area

3.2.2.3 Eutectic structure

In both the light and dark areas in XH-7 alloy a eutectic structure can be observed The main difference was the amount of eutectic phase larger in the dark areas when compared to the light one. This can be observed by comparing figure 11 and 16. This eutectic structure consists of:

- A grey phase which makes up the majority of the eutectic, this phase shows strong signals for iron, tungsten, chromium and carbon.
- A very fine darker phase, because of the fineness of this phase it is difficult to analyse the composition.

An image of this eutectic at high magnification can be seen in Figure 19 and an EDS mapping of this area can be seen in Figure 21. These images are taken from the SCA-H7 series, the cladding parameters for this series can be seen in Appendix 5.

When XH-7 is cladded using PTA the microstructure formed is coarser compared to laser cladded material. PTA cladded XH-7 is seen in Figure 22, in this image the same phases can be distinguished as in laser cladded XH-7 alloy.

1. The martensite matrix
2. The niobium carbide (FCC_A1#2)
3. The tungsten boride (M2B_tetr)
4. The grey eutectic

Because of the coarser structure however it can also be seen that the darker eutectic phase in this case are actually fine grains of matrix material: Martensite, ferrite or austenite. It is thought that this is also true for laser cladded XH-7.
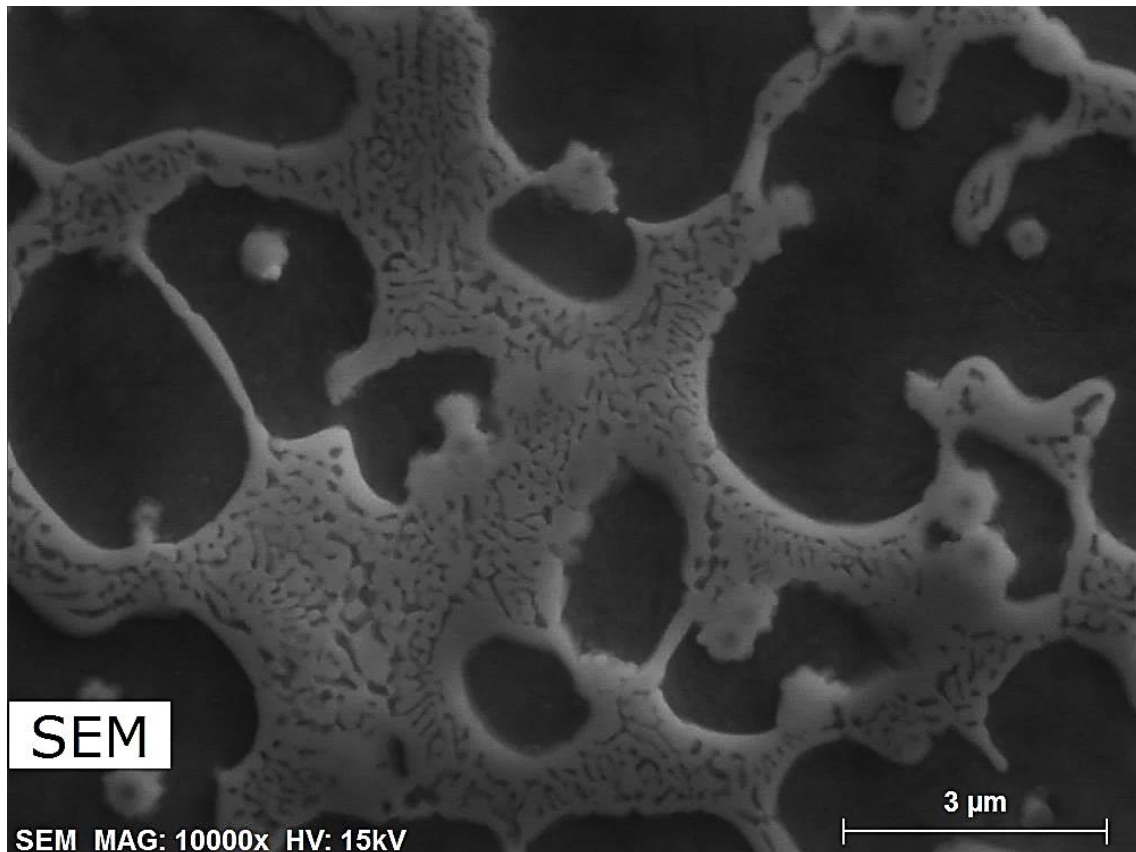
Figure 19. SCA-H7 close up of eutectic, etching in 3.3,
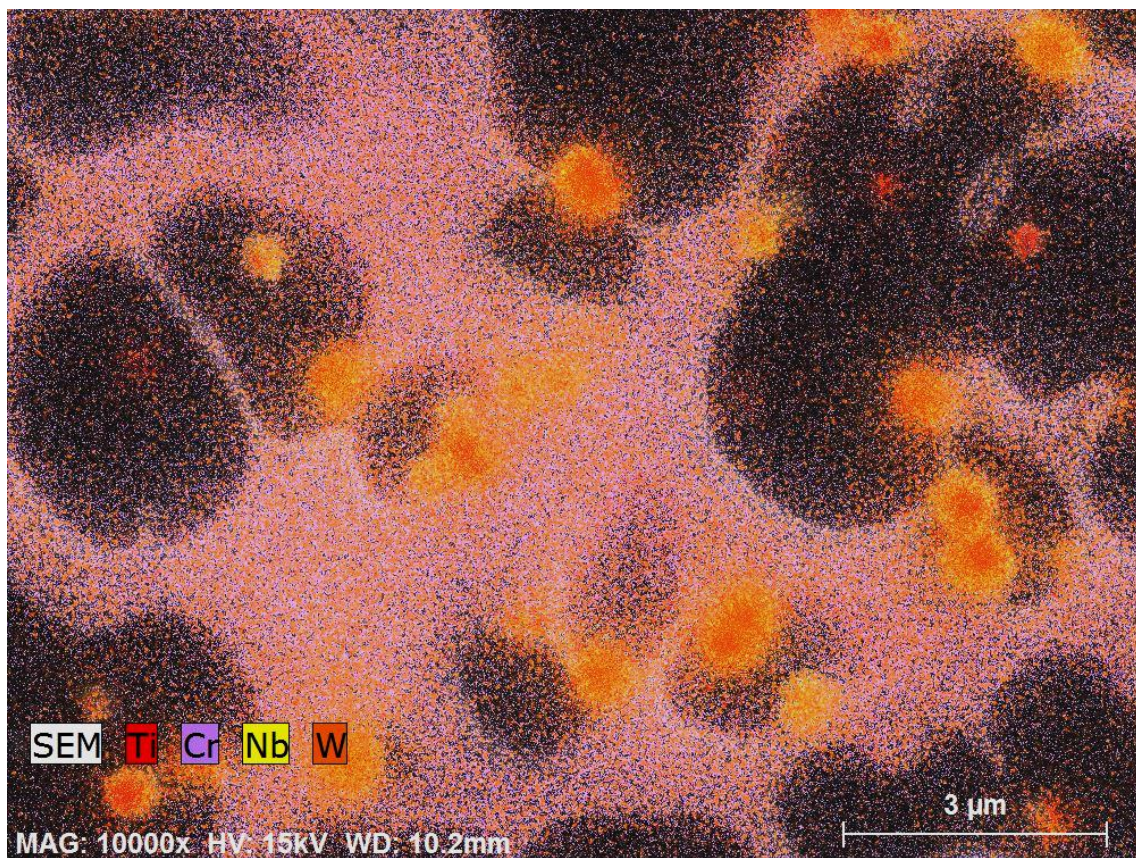
Figure 20. Figure 19 EDS map of Ti, Cr, Nb and W
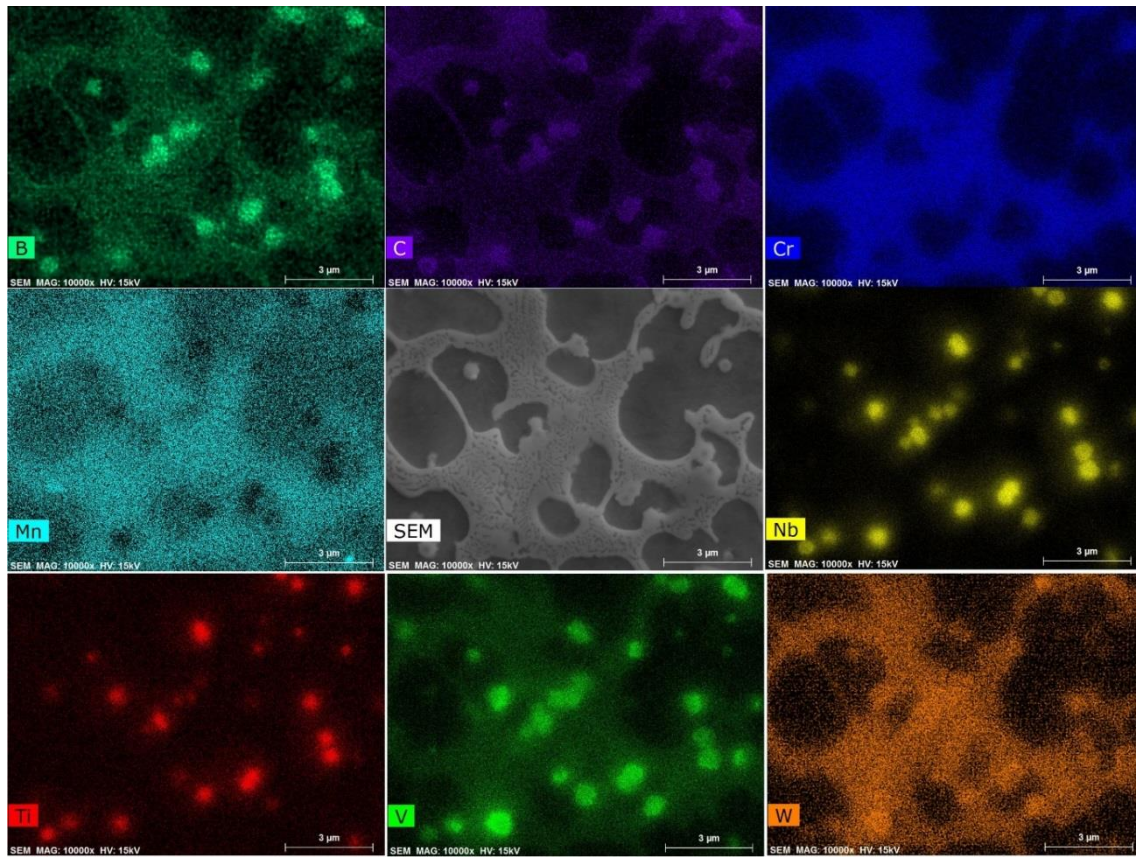
Figure 21. EDS mapping of Figure 19
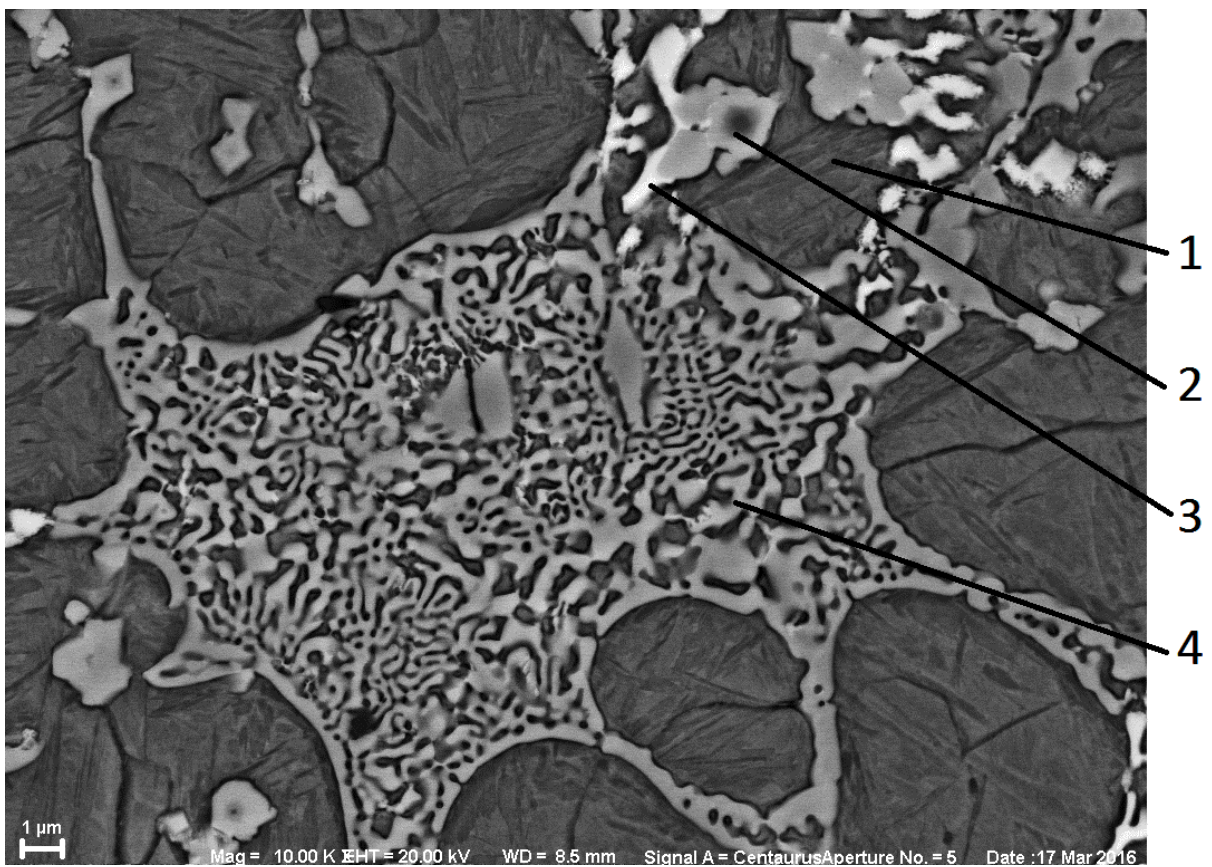
Figure 22. XH-7 PTA cladded XH-7, eutectic structure as seen under SEM

3.2.2.4 Hardness measurement

The result of the hardness measurement performed on the light and dark areas found in XH-7 alloy is shown in Table 8. These measurements show that the dark area is significantly softer than the light area.

Table 8. Hardness XH-7

Light area	Dark area
940 HV	600 HV

3.2.2.5 EBSD

In order to identify the matrix phase found in the dark areas found in XH-7 clads an EBSD analysis has been performed on two samples of this alloy. The results of this analysis is shown in Figure 23. The matrix is identified as having a BCC crystal structure. From this analysis it can be concluded that the matrix in the softer areas of XH-7 alloy is ferrite.
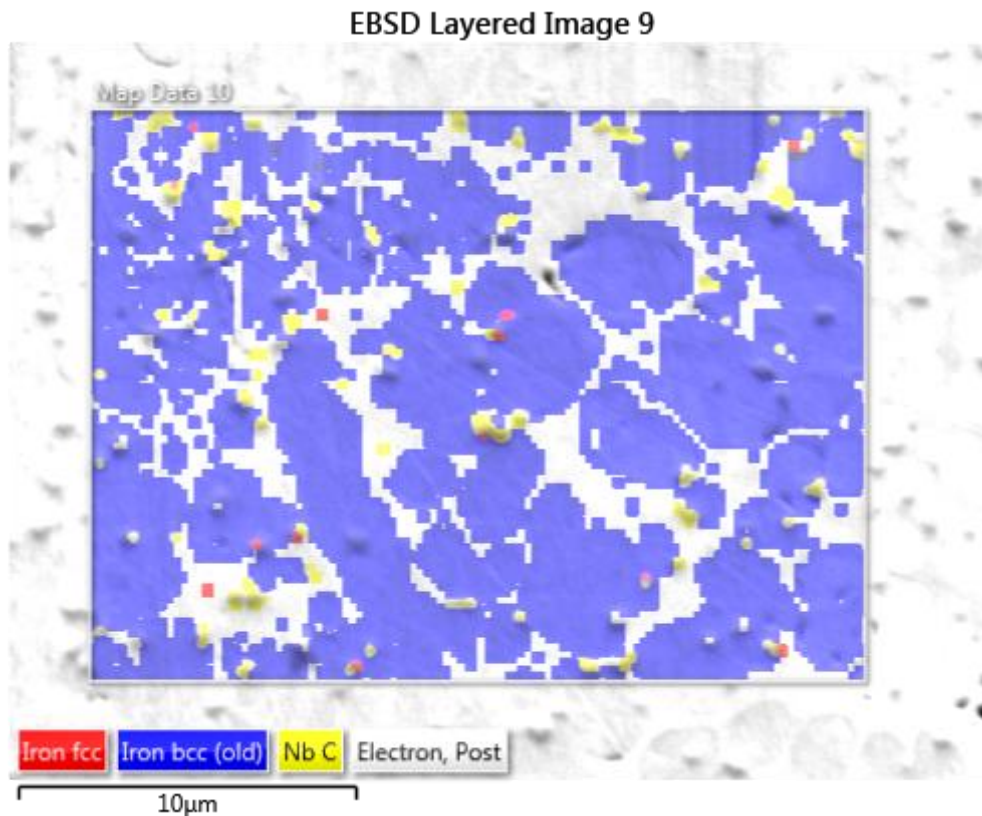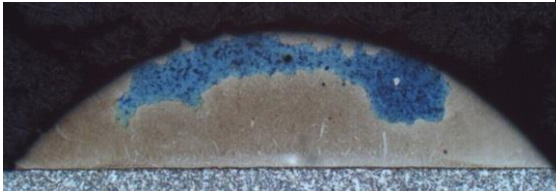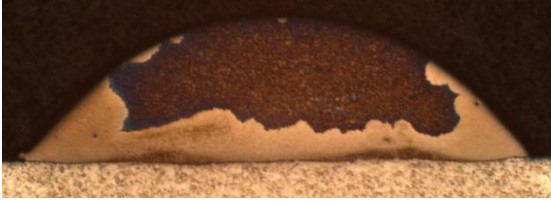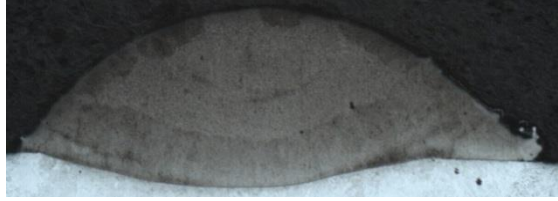
Figure 23. XH-7 laser cladded, sample N32 , etched in 3.3. EBSD analysis of dark area, showing a bcc crystallographic structure in the areas marked in blue, NbC (yellow).

3.2.3 Heat treatment

The results of the heat treatment experiment can be seen in Table 9.

Table 9. Microstructure of laser cladded XH-7 after heat treatment at 1000° C followed by cooling in furnace and in oil.

Sample	Before heat treatment	After heat treatment
N18		

N19		
N20		
N36		
N37		
N38		

The images in table 9 show that the dark area in all samples has become less distinct from the light area after heat treatment and etching despite the different cooling rates. It should be noted however that a difference is still visible.
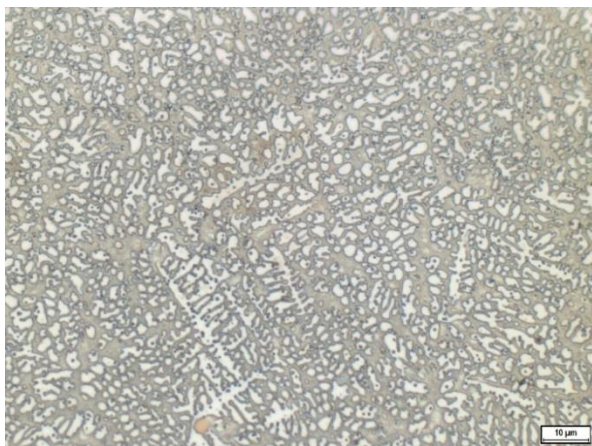
Figure 24. XH-7, sample N20, Etched in 3.3 Microstructure of the dark area before heat treatment.

Figure 25. XH-7, sample N20, Etched in 3.3 Microstructure of the dark area after heat treatment.

Figure 24 shows the microstructure of the dark area before heat treatment for sample N20, it can be seen that a white cellular/dendritic phase is present, also present are a grey eutectic phase, and carbides/borides. EBSD analysis performed at "Chalmers University of Technology"

has identified the white phase as ferrite, see EBSD. Figure 25 shows the dark area after heat treatment has been performed. The ferrite has been mostly replaced with martensite although some ferrite is still present. The amount of eutectic has decreased.
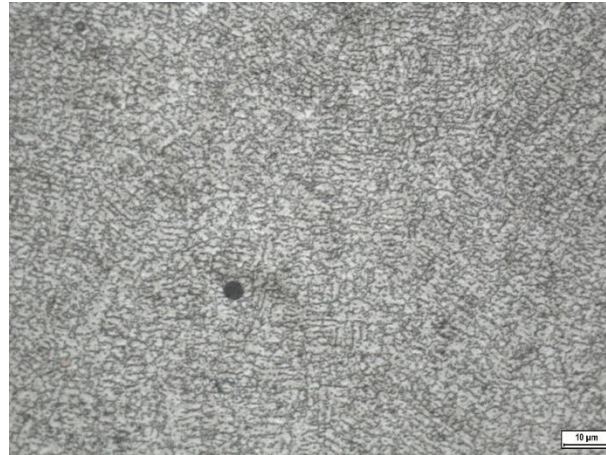
Figure 26. XH-7, sample N20, Etched in 3.3 Microstructure of the light area after heat treatment.

Figure 25 and Figure 26 show the microstructure of the dark and light areas after heat treatment. Figure 25 shows that the former dark area still contains some ferrite that is not present in the former light area. It also suggests that the ferrite is retained from before the heat treatment, since it has not formed in the light area.
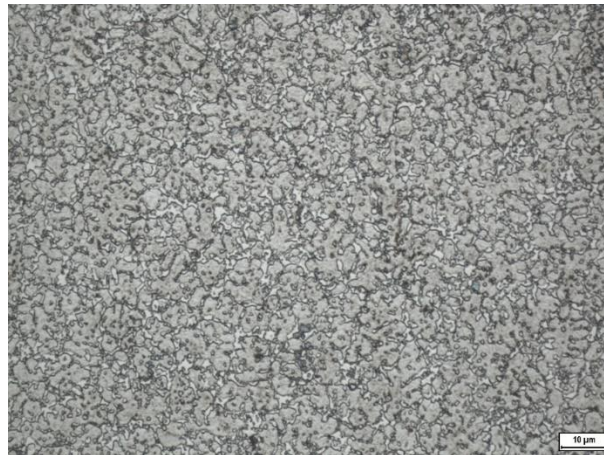
Figure 27. Dark area after heat treatment, oil quenched, sample N38

Figure 25 shows the dark area of sample N18 after heat treatment, and Figure 27 shows the dark area of sample N38 after heat treatment. For both samples the ferrite has transformed into a martensite matrix, both samples also contain remaining ferrite.

3.2.3.1 *Hardness measurement*

The hardness of the martensite in the samples has been tested after the heat treatment. The results of these measurements is shown in Table 10. The results in this table are an average of five measurements in an area. When compared with the results in Table 8 the measurements show an increase in hardness in the former soft area but a decrease in hardness in the former hard area. This difference in hardness could be the reason for the two areas can still be seen as separate areas in microscopy, since the etchant effected the softer area more than the harder area.

Table 10. of XH-7 former dark and light area observed after laser cladding after heat treatment, N36

Former dark area	Former light area
870HV	737HV

3.3 Discussion

From the information received in the simulations and the microstructure analysis a description of the solidification behaviour of the XH-7 material can be made.

Solidification of XH-7 begins around 1450°C with TiB_2. This is a very pure precipitate containing only titanium and boride.

At 1400°C a FCC carbide with a high niobium content but also high solubility of titanium, tungsten, and vanadium solidifies. In Figure 6, it can be seen that when this precipitate begins to form the amount of TiB_2 begins to decrease.

Figure 15 shows a line measurement performed across the diameter of this carbide showing an increase in titanium content in the centre. A similar result can be observed in Figure 14 where the titanium signal is concentrated in a more narrow area than the signal for niobium. For this reason, it is believed that this carbide uses the TiB_2 as a nucleation site.

At 1300°C the phase diagram predicts the formation of austenite while the Scheil diagram predicts the formation of ferrite. The metallographic analysis of the XH-7 material however shows that both phases are present. Austenite (transformed into martensite) forms in the faster cooling regions and the ferrite in the slower cooling area near the surface of the clad. In order to prove whether the ferrite could form through diffusional transformation from austenite the heat treatment experiment was performed. Here six clads were heated to austenitization temperature for one hour. Three samples were cooled rapidly in oil and three where cooled slowly in air. After heat treatment all these samples showed a martensitic matrix proving that even with slow cooling the austenite could transform into martensite and no solid state transformation of austenite into ferrite takes place. From this experiment it can be concluded that the ferrite phase forms directly from the liquid. In order to explain the formation of the ferrite two observations are made:

- The area with a ferrite matrix always forms near the surface, here the clad is cooled slowest. This should be the last area to solidify.
- Figure 8 shows that the solidification of the NbC decreases the carbon content in the liquid, with its lowest concentration right before solidification of the matrix begins at 1310°C.

Because of the higher cooling rate in the light area of the XH-7 clad it is possible that the austenite began solidifying before the NbC had time to sufficiently decrease the carbon content in the liquid.

At 1250°C a tungsten boride begins solidifying, this phase has a high content of iron, chromium, and vanadium. And if it formed near the NbC it also contains some niobium.

The phase diagram also predicts the formation of a vanadium based carbide with a high solubility of niobium, chromium and tungsten around 1150°C. This phase is not found in reality and instead the vanadium appears to be in solid solution in all the other phases. The absence of this phase is thought to be caused by the rapid cooling and low solidification temperature just before the solidus temperature.

Around 1100°C all liquid is solidified into a mixture of two phases through a eutectic reaction.

When the lighter eutectic phase is compared with the phase identified as M_2B_tetr, compositions in Table 6 and Table 7 it can be seen that they have a similar chemistry. For this reason this phase could actually be M_2B_tetr with a different chemistry caused by the

temperature and location at which it solidified. The difference between them is that the phase in the eutectic contains more iron and less niobium, and tungsten. The difference in iron and tungsten could be explained by the fact that the eutectic composition is done through an area measurement that also contains the darker phase, which is believed to be the matrix phase. It is thought that the grey phase found in the eutectic is M$_2$B_tetr that formed at the solidus this would correspond with results obtained in the Thermo-Calc simulation that shows a similar change in composition before and after the solidus at 1120°C of XH-7, as shown in Table 11. The reason the Chromium content does not change could again be explained by the addition of matrix phase in the measurements, bringing the average chromium content down.

Table 11. Composition change of M2B_tetr after solidus

Temperature	W	Fe	Cr	B
1200	66,9	24,8	3,6	4,7
1100	50,4	37,6	7,9	5,8

Another possible phase that could be formed in the eutectic reaction other than the M$_2$B_tetr is a M$_{23}$C$_6$. This phase is predicted by the Scheil diagram and if the altered liquid composition from Figure 9 is taken into account it can also form at the solidus according to the phase diagram. The simulated composition of this phase is shown in Table 12

Table 12. Simulated composition of M23C6, at 1000°C

Fe	Cr	C	B	Mn
86	7	3,5	1,6	1,1

3.4 Conclusion

When laser cladded the majority of the XH-7 material forms:
- A hard martensitic matrix containing fine carbide/boride precipitates and a eutectic structure.
- A smaller area normally near the surface of the clad, where the cooling rate is lower forms a softer ferritic matrix. This is caused by a combination of the lower cooling rate and depletion of the carbon content in the liquid due to the formation of carbides.

The heat treatment experiment shows that:
- Martensite start temperature is high enough to prevent ferrite formation even at slow cooling rates.
- The ferrite forms during solidification, instead of transforming from austenite during cooling.
- The soft area can be removed through heat treatment at 1000°C, however this solution is not desirable because the hardness of the coating remains uneven and processing time and costs are increased.

4 Phase 2

4.1 Experimental

In order to solve the problem of soft areas in XH-7 alloy, alternative compositions were developed. The strategy used while developing these alloys was making small changes to the XH-7 composition to influence specific properties to either provide information on the behaviour of the alloy or to provide a solution to the scatter of the microstructure. The goal of the developed alloys is shown in Table 13.

Before atomization the alloys have been simulated using Thermo-Calc.

Table 13. Goals set for the design of alternative alloys to XH-7

Alloy	Goal
XH-7A	Stabilize ferrite, increase soft area, increase amount of precipitates
XH-7B	Stabilize austenite
XH-7C	Stabilize austenite, increase martensite start

4.1.1 Process

The three alloys were atomised and sieved between 53 and 150µm to fulfil the requirement of the cladding equipment. Multiple clads of each powder were produced with varying laser cladding parameters in order to produce clads with different dilutions.
The parameters used can be found in:

XH-7A   Appendix 2
XH-7B   Appendix 3
XH-7C   Appendix 4

4.1.2 Materials

Alloy XH-7A was developed to increase area where ferrite is formed at high temperature. The alterations to the composition come at the expense of the iron content, the carbide/boride forming elements were kept constant.

Alloy XH-7B was developed to decrease the ferrite forming area and expand the area where austenite is stable. The alterations to the composition come at the expense of the iron content, the carbide/boride forming elements were kept constant.

Alloy XH-7C was developed to decrease the ferrite forming area and expand the area where austenite is stable. In order to prevent large amounts of retained austenite the martensite temperature is raised. The alterations to the composition come at the expense of the iron content, the carbide/boride forming elements were kept constant.

4.2 Results

4.2.1 XH-7A

The simulation of the phase diagram of alloy XH-7A is shown in Figure 28.

Figure 28. Phase diagram of alloy XH-7A, simulated using Thermo-Calc 3.1

When the phase diagram in Figure 28 is compared with the XH-7 phase diagram in Figure 5 the most important difference that can be seen is that for alloy XH-7A the ferrite forming area has been increased. The vertical black line shows the carbon content in XH-7A. It can be seen that unlike in normal XH-7 material this alloy will move through the ferrite forming area during solidification.

Figure 29 and Figure 30 show the etched cross-sections of a single track and a multiple track clad of XH-7A alloy.
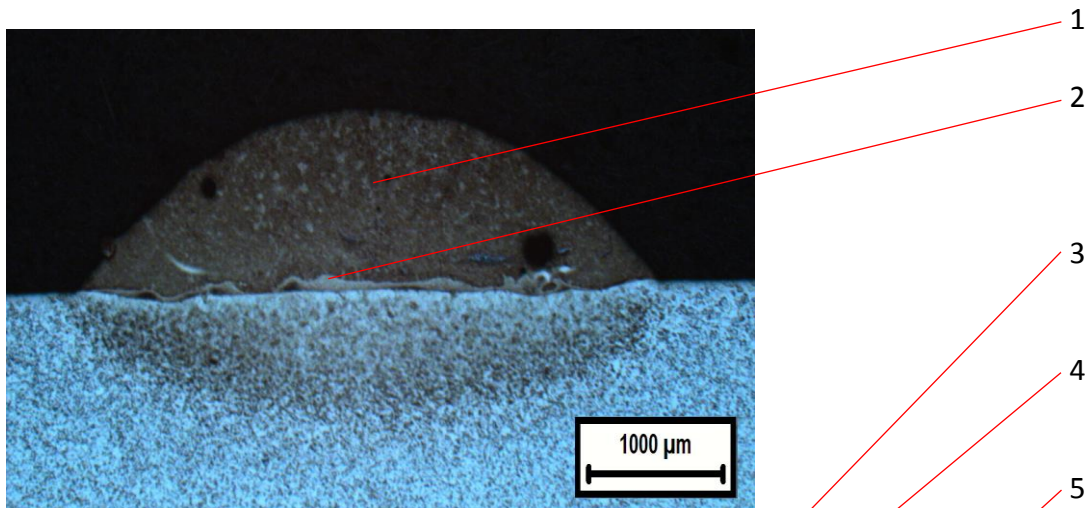
Figure 29. Laser cladded XH-7A, sample NHV1. Etched in 3.3. Overview of the coating cross section single track coating.

Figure 30. Laser cladded XH-7A, sample NHV17. Etched in 3.3. Overview of the coating cross section multitrack coating

In Figure 29 two areas can be distinguished:
1. Large dark area which covers most of the sample.
2. A thin light area along the interface with the substrate.

In Figure 30 three areas can be distinguished:

3. Large dark areas which cover most of the sample
4. A light area at the interface between clad and substrate
5. A band between two tracks which turn darker at the interface between two tracks.

Figure 31. Area 1 in Figure 29, Dark area in single track clad

Figure 32. Area 3 in Figure 30, Dark area in multitrack clad

Figure 31 and Figure 32 show the structure of the dark areas referred to as 1 and 3 in figures Figure 29 and Figure 30. It can be seen that in both cases this area consists mainly of a white phase, a eutectic, and there are also carbide and boride precipitates present. The white phase was identified as ferrite and the eutectic appeared to be a mix of carbides and borides. The

hardness measured in these areas is on average 569 HV. The relatively coarse orange particles in Figure 32 were identified as niobium carbides

Figure 33. Area 2 in Figure 29

Figure 34: Area 4 in Figure 30

Figure 33 and Figure 34 show the structure found in the interface between the clad and the substrate it can be seen that the ferrite found in the rest of the clad was replaced by martensite. The hardness measured in these areas is on average: 736HV
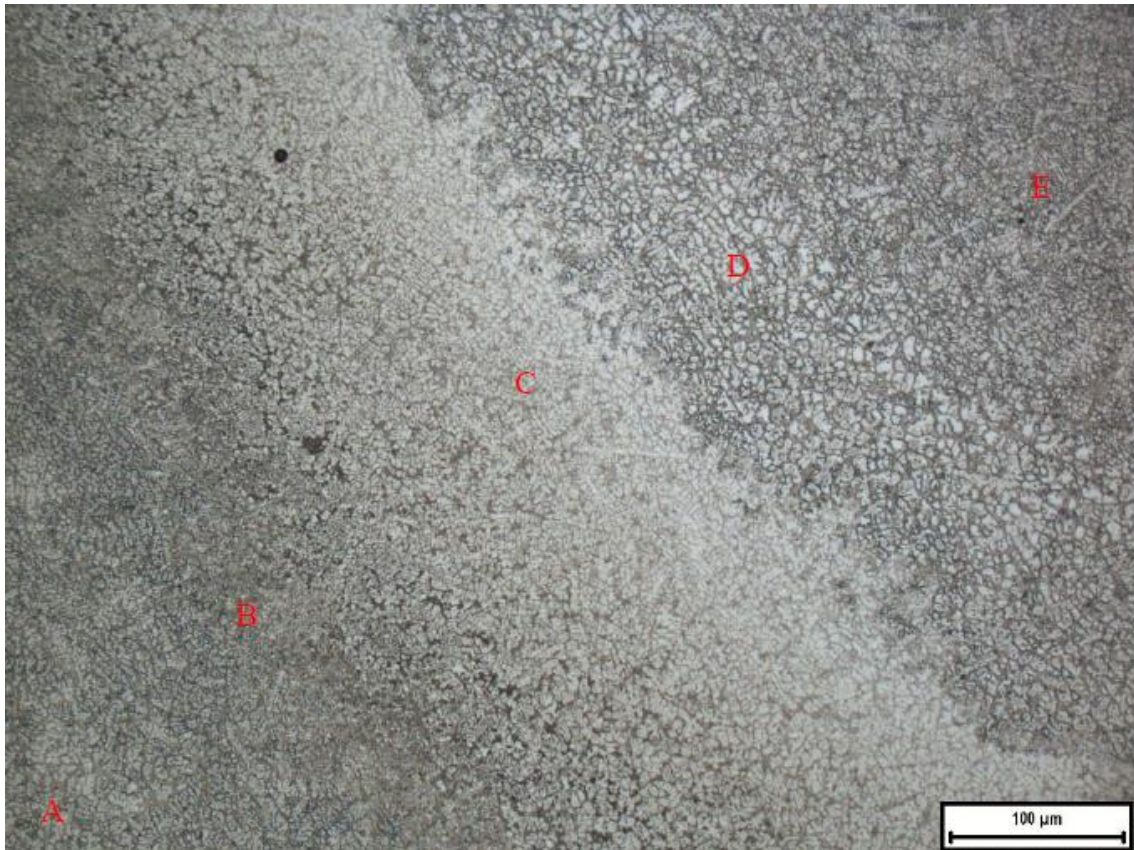
Figure 35: Close up of area 5 in Figure 30

Figure 35 shows the overlapping region between two tracks which looks like a white band at higher magnification. At higher magnification 5 different regions can be distinguished, which are designated area A to E.

A. Ferritic region of the pre-existing track
B. A martensitic region with a hardness of 881 HV
C. A region with fine ferrite with a hardness of 498 HV

38

D. A region with coarser ferrite than region C
E. The normal ferritic region of the newly made track

4.2.2 XH-7B

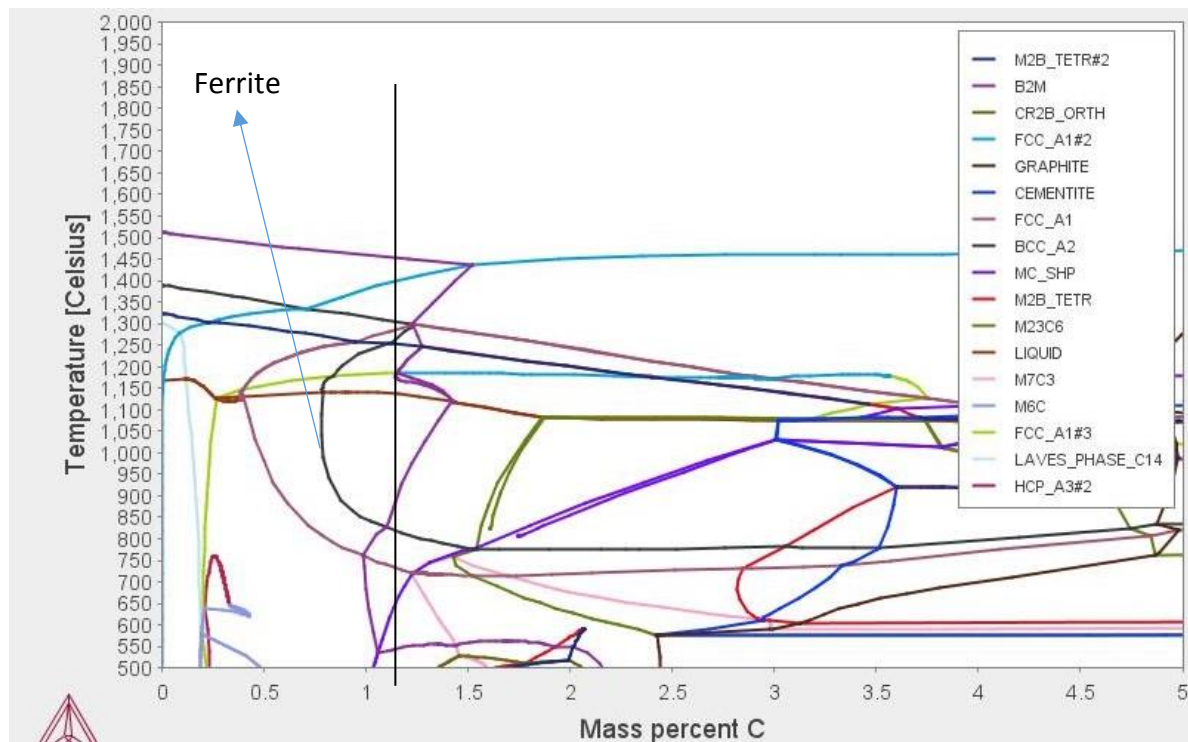The simulation of the phase diagram of alloy XH-7B is shown in Figure 36
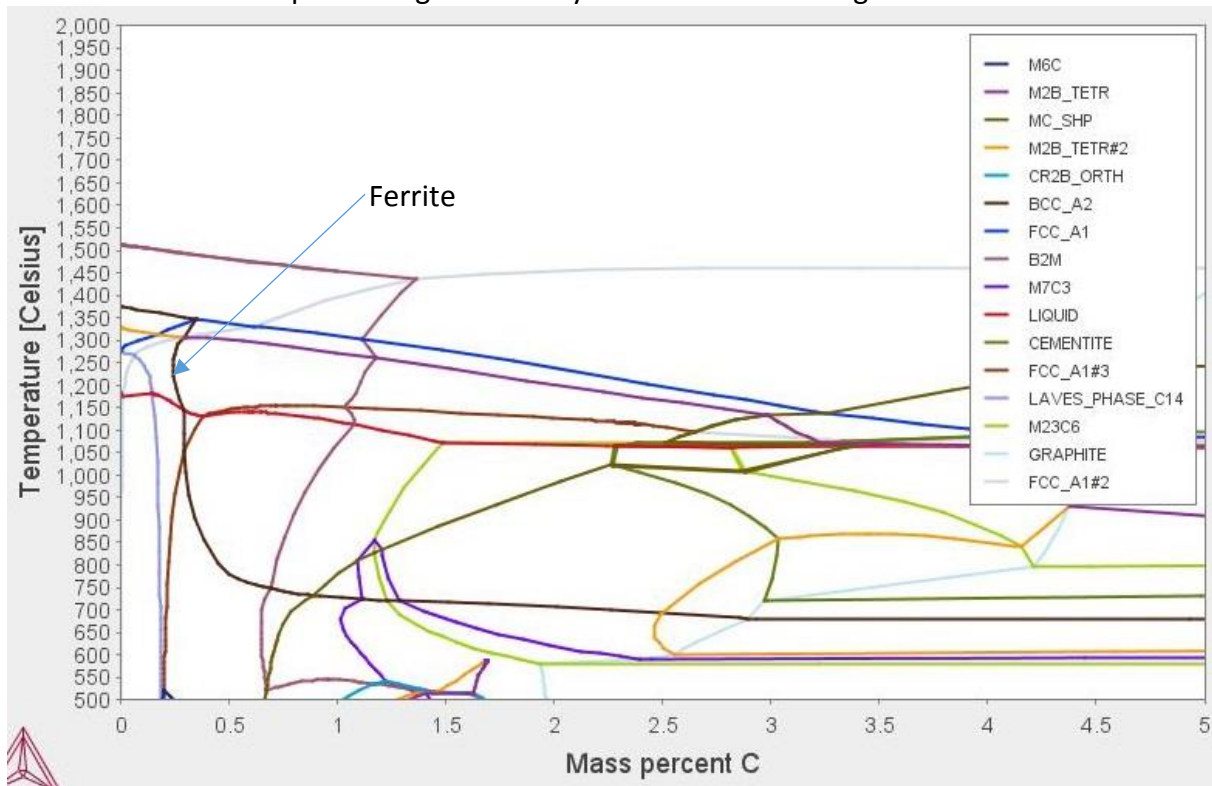
Figure 36. Phase diagram of alloy XH-7B, simulated using Thermo-Calc 3.1

When the phase diagram shown in Figure 36 is compared to the phase diagram of XH-7 in Figure 5 the most important difference is the decrease of the ferrite forming area. At high temperatures ferrite can start solidifying at 0,4% carbon. Because the ferrite forming area is pushed back compared to the original XH-7 it is expected that no ferrite will form. Because of the austenite stabilization effect of the alloying elements however there is a risk of some amount of retained austenite.

Figure 37 and Figure 38 show the etched cross-section of XH-7B clad. The primary phase is composed of martensite containing an amount of retained austenite. Also visible are a eutectic phase and small precipitates.

Figure 39 shows a higher magnification of the cross-section. In this image 5 phases can be seen:

Figure 40 shows the EDS mapping of this material

1. A martensitic phase consisting mainly of iron but also contains amounts of chromium, tungsten, niobium and silicon.
2. A lighter phase in the martensite which is not seen in the original XH-7 material. This phase is expected to be retained austenite caused by the addition of austenite stabilizing elements.
3. Dark particles with a grey shell. The EDS analysis shows that these particles show a strong signal of niobium and a slightly weaker signal for titanium. Combined with the information received from the Thermo-Calc simulation it is believed that this phase

first formed as titanium boride (B2M) which then acted as a nucleation site for niobium carbide ((FCC_A1#2).

4. A white intercellular/interdendritic phase consisting mainly of tungsten, with a contribution of chromium. This phase also shows a high signal for boron, which indicates a boride.

5. A grey eutectic structure containing high amounts of vanadium, tungsten, niobium and iron. This structure is made up of two different phases, but because of the fineness, the composition cannot accurately be measured separately. The two phases are described below

Figure 37. XH-7B sample 11

Figure 38. XH-7B, sample 11
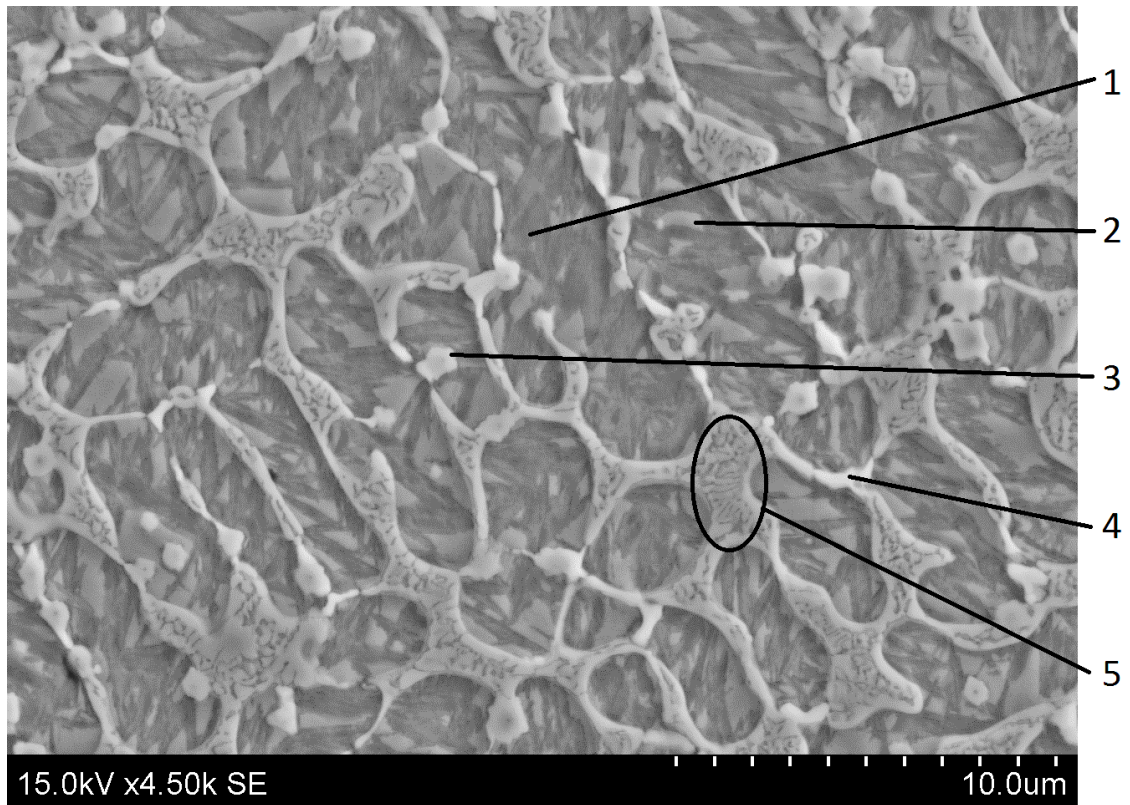
Figure 39. XH-7B, sample 12
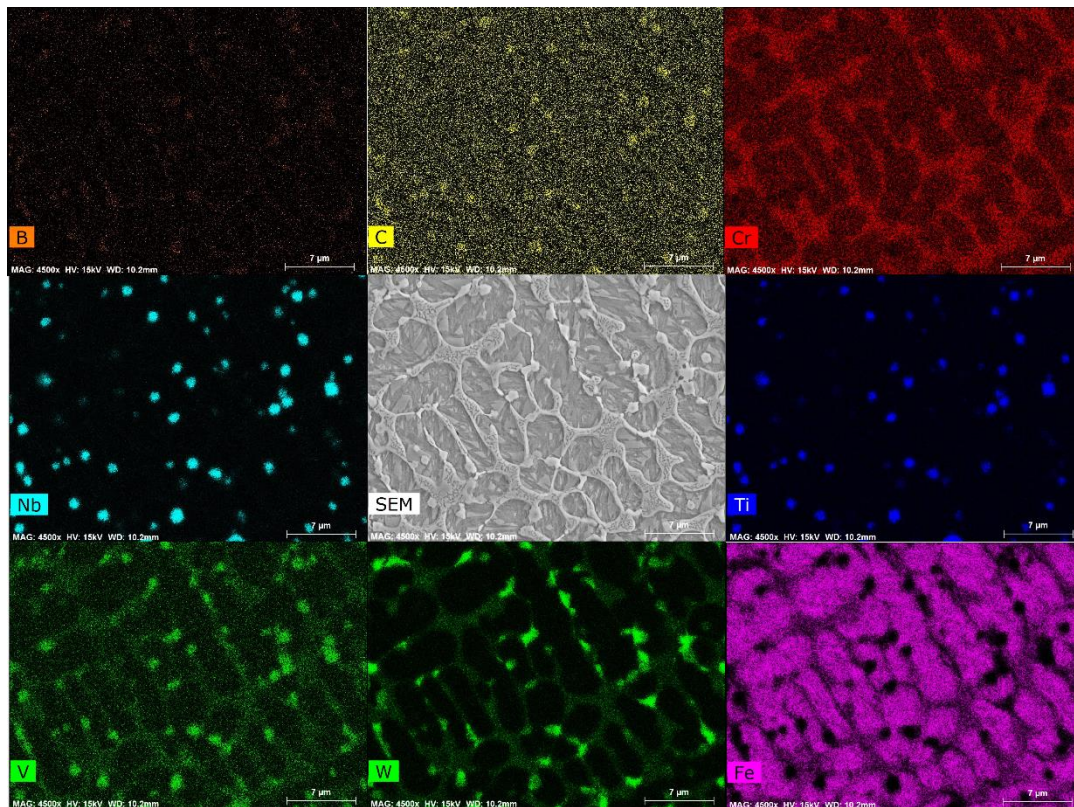
Figure 40. EDS mapping of Figure 39

Hardness measurements of the martensite matrix show that the hardness of this alloy is 852HV, this value is lower compared to the hard phase found in XH-7 material.

4.2.3 XH-7C

The simulation of alloy XH-7C is shown in Figure 41.
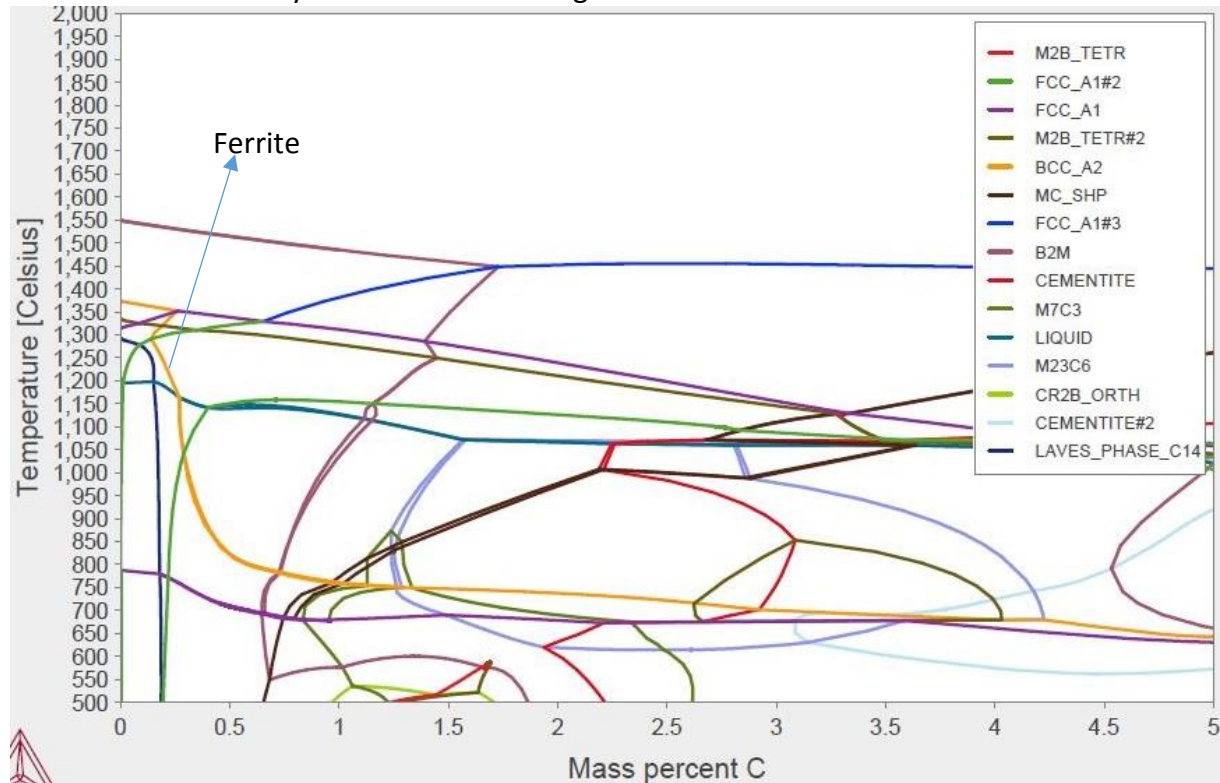
Figure 41. Phase diagram of alloy XH-7C

When the phase diagram shown in Figure 41 is compared to the phase diagram of XH-7 in Figure 5 the most important difference is the decrease of the ferrite forming area. At high temperatures ferrite can start solidifying at 0,3% carbon. Because the ferrite forming area is pushed back compared to the original XH-7 it is expected that no ferrite will form. Because of the austenite stabilization effect of the alloying elements however there is a risk of some amount of retained austenite. Compared to alloy XH-7B however the martensite start temperature is also raised, for this reason less retained austenite is expected in this alloy.

Figure 42 and Figure 43 show the etched cross-section of a XH-7C multitrack clad.

Figure 44 shows a higher magnification of the cross-section. In this image 5 phases can be seen

1. A martensitic phase consisting mainly of iron but also contains amounts of chromium, tungsten, niobium and silicon.
2. A lighter phase in the martensite which is not seen in the original XH-7 material. This phase is expected to be retained austenite caused by the addition of austenite stabilizing elements.
3. Dark particles with a grey shell. The EDS analysis shows that these particles show a strong signal of niobium and a slightly weaker signal for titanium. Combined with the information received from the Thermo-Calc simulation it is believed that this phase first formed as titanium boride (B2M) which then acted as a nucleation site for niobium carbide ((FCC_A1#2).
4. A white intercellular/interdendritic phase consisting mainly of tungsten, with a contribution of chromium. This phase also shows a high signal for boron, which indicates a boride.

42

5. A grey eutectic structure containing high amounts of vanadium, tungsten, niobium and iron. This structure is made up of two different phases, but because of the fineness, the composition cannot accurately be measured separately. The two phases are described below

*Figure 42. XH-7C, sample 12, etching in 3.3, Overview of the coating cross section showing an even microstructure in the coating*

Figure 43. XH-7C, sample 11, etching in 3.3, close up of clad cross section
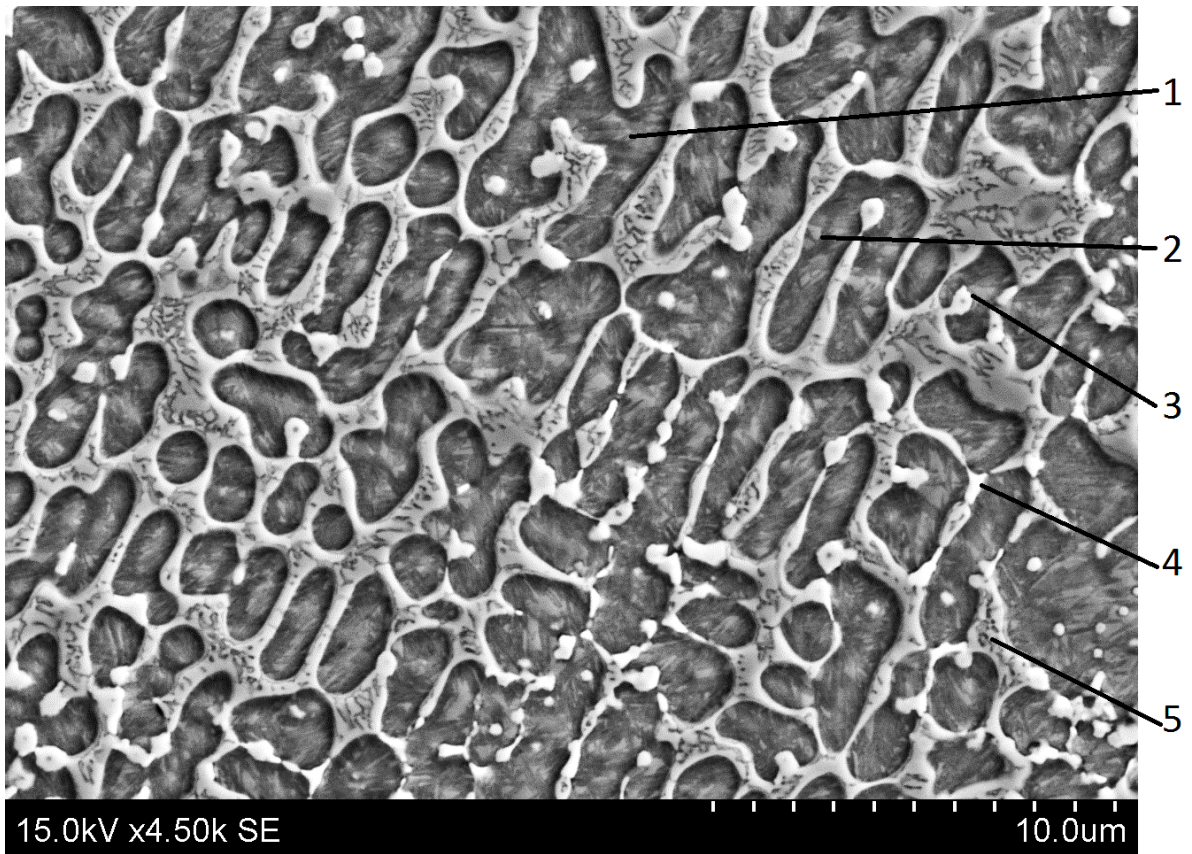
Figure 44. XH-7C, sample 12

4.3 Discussion

4.3.1 XH-7A

Laser cladded XH-7 material shows scatter of the microstructure in the coating. The microstructure of the matrix material can change from martensite to ferrite within the same clad resulting in the formation of a hard and soft area with a martensitic and ferritic matrix respectively. The heat treatment experiment described in the first phase of this report has shown that the ferrite in these clads is formed during solidification. However, the phase diagram, Figure 5, predicts the formation of austenite. The Scheil diagram on the other hand predicts that solidification begins with ferrite, Figure 7.

It is possible that the solidification of carbide precipitates depletes the carbon content of the liquid enough that a full ferritic matrix is formed first during solidification which then transforms into austenite during cooling, in this case the soft area would be ferrite that has not had the time to transform into austenite. In order to examine whether this transformation is possible alloy XH-7A was developed with enough BCC stabilizing elements to allow solidification to begin with ferrite and then transition into the austenite forming region during cooling, as shown in Figure 28. If the transformation is possible the cross section of the clad should show an area with either a martensitic or austenitic matrix.

Figure 29 to Figure 35 show that the matrix phase formed by this alloy after laser cladding is nearly completely ferritic. There are also two regions were martensite is found:

1. The interface between the substrate material. Figure 45 shows that the size of this area increases with increasing dilution. Therefore, the formation of the austenite/martensite in this area is probably favoured by the dilution of the chemistry.
2. The interface between the tracks. This can be seen in Figure 35 in the region designated as B. The martensite in this region is probably formed when the ferrite in a pre-existing track is heated to austenitization temperature (Figure 28, 800 to 1250°C) when the neighboring track is being deposited, this austenite then transforms into martensite when quenching occurs as the heat source moves away.

From this it can be concluded that the cooling rate during laser cladding is too high for diffusional transformation to occur.
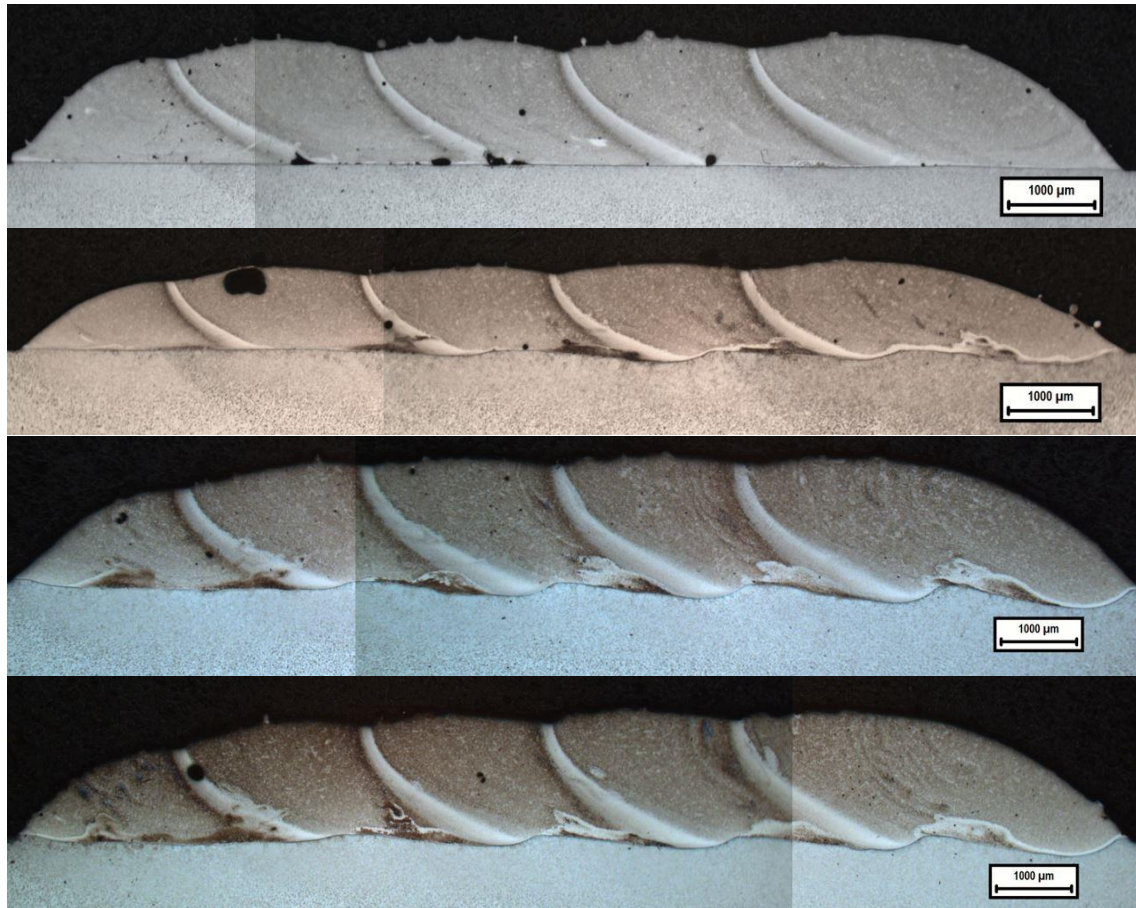
Figure 45. dilution in different samples 2, 4, 6 & 8 of the NHV series in Appendix 2

4.3.2 XH-7B

When laser cladded the XH-7B alloy does not form soft areas. Hardness measurements of the matrix phase have shown that with a hardness of 852HV the hardness of this material is lower than the matrix phase found in the hard area of the original material (940HV). This lowered hardness is probably caused by the presence of retained austenite.

Retained austenite is formed when austenite is not quenched to the martensite finish (M_f) temperature. The presence of retained austenite is not always undesirable. Effects of retained austenite are [7]:

- Lowered hardness
- Lowered dimensional stability: Martensite (BCC) has a greater volume than austenite (FCC). As austenite transforms there will be a local volume increase of 4-5%, if the amount of retained austenite is high enough this can lead to dimensional changes and in the worst case crack initiation.
- Increased fatigue strength: Due to retained austenite's ductility it can blunt the tip of cracks as they form which delays crack growth. Another way retained austenite can prevent crack formation is by the compressive stresses formed as it transforms into martensite when stresses are applied. These stresses counteract the tensile stresses formed at the crack tip required for further crack growth.
- Impact resistance: Austenite is tougher and has higher impact resistance than martensite, having some retained austenite is beneficial for this mechanical property.

The reason no ferrite is formed in this material can be seen in the phase diagram in Figure 36. In this phase diagram it can be seen that the ferrite forming region is pushed back and the

area were the niobium carbide (FCC_A1#2) is formed intersects with the austenite forming area before reaching the ferrite forming area. In the XH-7 phase diagram this is reversed. It is believed that this, in combination with the high cooling rate from laser cladding, makes it impossible for the formation of NbC to decrease the carbon content of the liquid enough to allow for the formation of ferrite before a fully austenitic matrix is solidified.

4.3.3 XH-7C

When laser cladded the XH-7C alloy does not form soft areas. Hardness measurements of the matrix phase have shown that with a hardness of 991HV the hardness of this material is similar to the matrix phase found in the hard area of the original material (940HV). The material shows a similar microstructure as XH-7B though with less retained austenite and a finer grain size.

When comparing the phase diagrams XH-7C has a stronger effect on the suppression of the ferrite forming region than XH-7B. XH-7C is also harder than XH-7B, this increase in hardness is caused by the increase of the martensite start temperature which results in less retained austenite.

4.4 Conclusion

Metallographic analysis of XH-7A in combination with the conclusions of the heat treatment experiment in the first phase of this thesis has shown that the austenitic(martensitic) and ferritic matrix both solidify directly from the liquid without solid state transformations occurring. Alloy XH-7A has also shown that an increase of the delta-ferrite forming area will result in a nearly complete ferritic matrix when laser cladded. Because of the fully ferritic matrix this material shows a lower hardness than the original XH-7 material.

Metallographic analysis of XH-7B has shown that stabilization of austenite results in a martensitic matrix with high amounts of retained austenite when laser cladded. This alloy shows a lower hardness than the original XH-7 material due to the presence of retained austenite. Despite the lowered hardness this alloy could show better properties in fatigue strength and impact resistance, although this would need to be analysed further.

Metallographic analysis of XH-7C has shown that stabilization of austenite and an increased martensite start temperature results in a martensitic matrix with similar hardness as the original XH-7 material when laser cladded. XH-7C does not show scatter in the microstructure like the one found in the original XH-7 material when laser cladded.

5 Further work

In this chapter several topic of possible future research on the XH-7 material are given.

- Further testing of mechanical properties: In this thesis mechanical testing has been focused in hardness analysis. Further mechanical testing could be done on wear and impact resistance, and adhesive properties.
- Desirability of retained austenite in the discussion chapter it was said that retained austenite is not always undesirable. The desirability of retained austenite could be tested by comparing the properties of XH-7B and XH-7C.
- Amount of alloying necessary to prevent ferrite formation: Alloys XH-7B and XH-7C both resolve the issue of irregular hardness found in laser cladded XH-7. These alloys were developed with an overabundance of the alloying elements required to achieve the goal of the material.
- Heat treatment of alloy XH-7A: The XH-7A alloy shows a fully ferritic matrix, in earlier heat treatment experiments it was shown that when heat treated the ferritic matrix forms a martensitic matrix with lowered hardness to the original XH-7. It could be of interest to examine the effect of heat treatment on the XH-7A material.

6 Bibliography

[1]   ASTM-A600, ASTM, 2004.

[2]   C. Højerslev, "Tool Steels," Risø National Laboratory, roskilde, 2001.

[3]   D. Porter and K. Easterling, Phase transformations in metals and alloys, wokingham: Van Nostrand Reinhold, 1992.

[4]   K. Ishida, "Calculation of the effect of alloying elements on the Ms temperature in steels," *Journal of Alloys and Compounds,* no. 220, pp. 126 - 131, 1995.

[5]   J. Milewski and T. Palmer, "ASM Handbook Vol 6A, Welding Fundamentals and Processes, Laser Deposition Processes, Laser Cladding," ASM International, 2011, p. 587–594.

[6]   M. Schneider, "Laser cladding with powders," University of Twente, Twente, 1998.

[7]   G. Thomas, "Retained Austenite and Tempered Martensite Embrittlement," *American society for metals and the metalurgical society of Aime,* vol. 9A, no. 439, 1978.

[8]   H. Gedda, "Laser cladding: An experimental and theoretical investigation," Luleå Universtity of technology, Luleå, 2004.

[9]   G. Krauss, "ASM Handbook Vol 1, , Properties and Selection: Irons, Steels, and High-Performance Alloys, Microstructures, Processing, and Properties of Steels, Martensite," ASM international, 1990, pp. 126 - 139.

[10] A. M. Bayer, B. A. Becherer and T. Vasco, "ASM Handbook vol 16, Machining, High-speed tool steels," ASM international, 1989, pp. 51-59.

[11] R. M. Deacon, ASM handbook, volume 9, Metallography and Microstructures, Martensitic Structures, ASM international, 2004.

[12] T. N. Baker, "Processes, microstructure and properties of vanadium microalloyed steels," *Materials Science and Technology,* pp. Vol 25, No 9, 2009.

Appendix 1

N series XH-7 trial

Material: XH-7

Cladding equipment: Laser cladded at Nutch GMBH using a 6kW IPG laser with a 5mm spot size.

Sample	Laser power [W]	Speed [mm/sec]	Feed rate [g/min]	Spot size [mm]	Tracks	Layers
N1	2500	16	30	5	1	1
N2	2300	16	30	5	1	1
N3	2100	16	30	5	1	1
N4	2700	16	30	5	1	1
N5	2900	16	30	5	1	1
N6	2500	16	30	5	1	1
N7	2500	16	30	5	5	1
N8	2700	16	30	5	5	1
N9	2300	16	30	5	5	1
N10	2100	16	30	5	5	1
N11	1500	8	18	5	5	1
N12	1500	16	30	5	1	1
N13	1700	16	30	5	1	1
N14	1900	16	30	5	1	1
N15	2100	16	30	5	1	1
N16	2300	16	30	5	1	1
N17	2500	16	30	5	1	1
N18	2700	16	30	5	1	1
N19	2900	16	30	5	1	1
N20	3100	16	30	5	1	1
N21	3300	16	30	5	1	1
N22	3500	16	30	5	1	1
N23	3700	16	30	5	1	1
N24	2500	16	30	5	5	1
N25	2700	16	30	5	5	1
N26	2900	16	30	5	5	1
N27	700	8	18	5	1	1
N28	900	8	18	5	1	1
N29	1100	8	18	5	1	1
N30	1300	8	18	5	1	1
N31	1500	8	18	5	1	1
N32	1700	8	18	5	1	1
N33	1900	8	18	5	1	1
N34	2100	8	18	5	1	1
N35	2300	8	18	5	1	1
N36	2500	8	18	5	1	1
N37	2700	8	18	5	1	1
N38	2900	8	18	5	1	1
N39	3100	8	18	5	1	1
N40	3300	8	18	5	1	1

N41	3500	8	18	5	1	1
N42	2100	8	18	5	5	1
N43	1900	8	18	5	5	1
N44	1700	8	18	5	5	1
N45	1500	8	18	5	5	1
N46	1700	8	18	5	5	1
N47	1500	8	18	5	5	1
N48	1500	8	12	5	5	1
N49	1500	8	12	5	5	1
N50	1500	10	12	5	5	1
N51	1800	12	14.5	5	5	1

Appendix 2

NHV series

Material: XH-7A

Cladding equipment: Laser cladded at Nutch GMBH using a 6kW IPG laser with a 5mm spot size.

Sample	Laser power [W]	Speed [mm/sec]	Feed rate [g/min]	Spot size [mm]	Tracks	Layers
NHV1	2700	16	29,8	5	1	1
NHV2	2700	16	29,8	5	5	1
NHV3	3100	16	29,8	5	1	1
NHV4	3100	16	29,8	5	5	1
NHV5	3300	16	29,8	5	1	1
NHV6	3300	16	29,8	5	5	1
NHV7	1500	8	18	5	1	1
NHV8	1500	8	18	5	5	1
NHV9	1500	8	12	5	1	1
NHV10	1500	8	12	5	5	1
NHV11	1200	5	12	5	1	1
NHV12	1500	5	12	5	1	1
NHV13	1650	5	12	5	1	1
NHV14	1650	5	12	5	1	1
NHV15	1500	5	12	5	1	1
NHV16	1500	5	12	5	1	1
NHV17	1500	5	12	5	5	1
NHV18	1650	5	12	5	1	1
NHV19	1650	5	12	5	5	1

Appendix 3

XH-7B series
Material: XH-7B
Cladding equipment: Laser cladded at Nutch GMBH using a 6kW IPG laser with a 5mm spot size.

Sample	Laser power [W]	Speed [mm/sec]	Feed rate [g/min]	Spot size [mm]	Tracks	Layers
H7B1	1000	16	29.6	5	1	1
H7B2	1500	16	29.6	5	1	1
H7B3	2000	16	29.6	5	1	1
H7B4	2500	16	29.6	5	1	1
H7B5	3000	16	29.6	5	1	1
H7B6	3500	16	29.6	5	1	1
H7B7	4000	16	29.6	5	1	1
H7B8	4500	16	29.6	5	1	1
H7B9	5000	16	29.6	5	1	1
H7B10	3500	16	29.6	5	5	1
H7B11	4000	16	29.6	5	5	1
H7B12	4500	16	29.6	5	5	1

Appendix 4

XH-7C series
Material: XH-7C
Cladding equipment: Laser cladded at Nutch GMBH using a 6kW IPG laser with a 5mm spot size.

Sample	Laser power [W]	Speed [mm/sec]	Feed rate [g/min]	Spot size [mm]	Tracks	Layers
H7C1	1000	16	30.9	5	1	1
H7C2	1500	16	30.9	5	1	1
H7C3	2000	16	30.9	5	1	1
H7C4	2500	16	30.9	5	1	1
H7C5	3000	16	30.9	5	1	1
H7C6	3500	16	30.9	5	1	1
H7C7	4000	16	30.9	5	1	1
H7C8	4500	16	30.9	5	1	1
H7C9	5000	16	30.9	5	1	1
H7C10	3000	16	30.9	5	5	1
H7C11	3500	16	30.9	5	5	1
H7C12	4000	16	30.9	5	5	1

Appendix 5

SCA-H7 series
Material: XH-7
Cladding equipment: Laser cladded at Nutch GMBH using a 6kW IPG laser with a 5mm spot size

Sample	Laser power [W]	Speed [mm/sec]	Feed rate [g/min]	Spot size [mm]	Tracks	Layers
H7-1	1000	16	30.9	5	1	1
H7-2	1500	16	30.9	5	1	1
H7-3	2000	16	30.9	5	1	1
H7-4	2500	16	30.9	5	1	1
H7-5	3000	16	30.9	5	1	1
H7-6	3500	16	30.9	5	1	1
H7-7	4000	16	30.9	5	1	1
H7-8	4500	16	30.9	5	1	1
H7-9	5000	16	30.9	5	1	1
H7-10	3000	16	30.9	5	5	1
H7-11	3500	16	30.9	5	5	1
H7-12	4000	16	30.9	5	5	1
H7-13	4500	16	30.9	5	5	1